CHALMERS
UNIVERSITY OF TECHNOLOGY

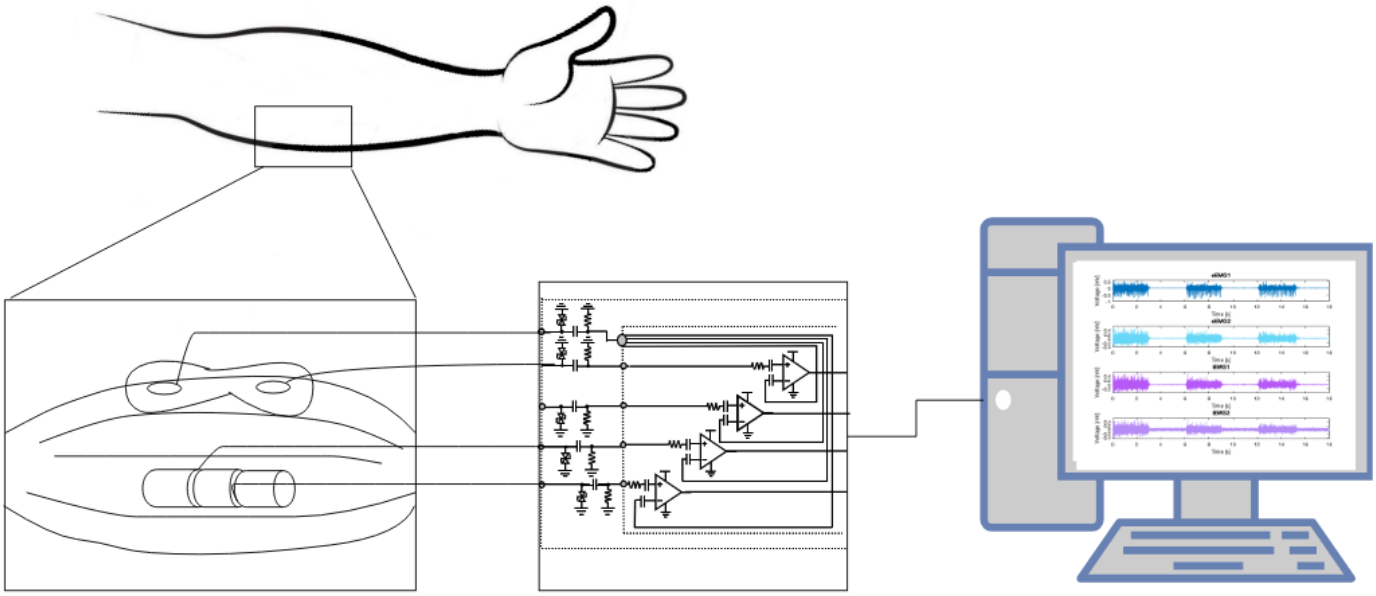

Electromyography Recordings with Epimysial and Intramuscular Electrodes

Master's Thesis in Biomedical Engineering

Berglind Hlidkvist Thorgeirsdottir

Department of Electrical Engineering
Division of Signal Processing and Biomedical Engineering
Biomechatronics and neurorehabilitation laboratory
CHALMERS UNIVERSITY OF TECHNOLOGY
Gothenburg, Sweden 2019
Master's Thesis 2019

MASTER'S THESIS 2019

Electromyography Recordings with Epimysial and Intramuscular Electrodes

Master's Thesis in Biomedical Engineering

Berglind Hlidkvist Thorgeirsdottir

Department of Electrical Engineering

Division of Signal Processing and Biomedical Engineering

Biomechatronics and neurorehabilitation laboratory

CHALMERS UNIVERSITY OF TECHNOLOGY

Gothenburg, Sweden 2019

Electromyography Recordings with Epimysial and Intramuscular Electrodes
Master's Thesis in Biomedical Engineering

Berglind Hlidkvist Thorgeirsdottir

Supervisors: Dr. Max Ortiz-Catalan and Dr. Enzo Mastinu, Department of Electrical Engineering, Chalmers University of Technology.
Examiner: Dr. Max Ortiz Catalan, Associate Professor, Department of Electrical Engineering.

Department of Electrical Engineering
Division of Signal Processing and Biomedical Engineering
Biomechatronics and neurorehabilitation laboratory
Chalmers University of Technology
SE-412 96 Gothenburg
Sweden
Telephone: + 46 (0)31-772 1000

Typeset in Microsoft Word
Gothenburg, Sweden, 2019

Electromyography Recordings with Epimysial and Intramuscular Electrodes

Master's thesis in Biomedical Engineering

Berglind Hlidkvist Thorgeirsdottir
Department of Electrical Engineering
Division of Signal Processing and Biomedical Engineering
Biomechatronics and neurorehabilitation laboratory
Chalmers University of Technology

ABSTRACT

Electromyography (EMG) is the recording of the electrical activity produced during muscular contractions. EMG is most commonly acquired via electrodes placed on the surface of the skin above muscle of interest (sEMG), and this is the preferred method for control of powered upper limb prostheses. Implanted electrodes over or inside muscles provide higher quality signals than sEMG. However, little is known about the performance of these extra- and intra-muscular electrodes types against each other.

The objective of this study was to design an experimental procedure to compare two types of implanted muscular electrode for EMG recordings, namely intramuscular (iEMG) and epimysial (eEMG).

A framework for evaluation of iEMG and eEMG electrodes with regards to signal to noise ratio (SNR) was developed. The experimental procedure was tested by implanting each type of these electrodes in the Flexor Carpi Ulnaris (FCU) muscle of a volunteer. The volunteer was instructed to perform ten selective movements to generate EMG signals. The EMG signals were acquired, simultaneously from both electrode types, using three different analog front ends (AFEs), and via an open-source platform for myoelectric pattern recognition (BioPatRec). In addition to SNR, crosstalk between adjacent muscles and myoelectric pattern recognition (MPR) accuracy was compared between electrode types and recording systems.

The results from this single case study indicated that eEMG outperforms iEMG based on the aforementioned metrics. However, further work using the methods developed in this study must be done to reach conclusive results.

Keywords: Electromyography, intramuscular electrodes, epimysial electrodes, analog front end, data acquisition, signal to noise ratio, crosstalk, myoelectric pattern recognition.

ACKNOWLEDGMENTS

I want to thank my supervisors Prof. Max Ortiz Catalan and Dr. Enzo Mastinu for all the help and guidance through this thesis. I will always be grateful for the opportunity to work with such an exciting topic in my field of interest.

The Biomechatronics and Neurorehabilitation Laboratory (BNL) was a great place to be due to the people around, special thanks to Bahare Ahkami, Autumn Naber, Jan Zbinden and Maria Muñoz for their help. Thanks to my fellow master's thesis students Linn Berntsson, Tryggvi Kaspersen, and Daniel Fridolfsson for all the long hours in the lab.

I am very thankful for the opportunity to work partly at Integrum AB. It was a great experience to be there and get to know all the fantastic people that work hard every day to improve the life of amputees. Andrej Litvin and Wafa Tigra were of great help with any questions I had; for that, I am incredibly grateful.

For proofreading my thesis and going through this with me, special thank you to Bryndís Hjörleifsdóttir and Anoop Subramanian.

To all my friends I have made here over the last two years, could not have had better group of people around me.

To my family I will be forever grateful for all the sacrifices and the support you have given me.

Berglind Hlidkvist Thorgeirsdottir, Gothenburg, September 2019

Contents

Acronyms and Abbreviations

MPR	Myoelectric Pattern Recognition.
EMG	Electromyography.
MES	Myoelectric Signals.
iEMG	Intramuscular Electromyography.
eEMG	Epimysial Electromyography.
sEMG	Surface Electromyography.
SNR	Signal to Noise Ratio.
LDA	Linear Discriminant Analysis.
AFE	Analog Front End.
ADC	Analog to Digital Conversion.
AC	Alternating Current.
MVC	Maximum Voluntary Contraction.
RMS	Root Mean Square.
GUI	Graphical User Interface
DOI	Date of Implantation
DOE	Date of Ex-plantation

1 Introduction

The number of people suffering from limb loss is rapidly increasing. In the year 2005, an estimated 1.6 million people in the United States suffered from limb loss. It is estimated that this number will double before 2050 [1]. Primarily due to the rising prevalence of vascular diseases, i.e., caused or acquired from the poor vascular circulation of a limb. This predicted increase demands viable and affordable alternatives to limb replacement. The options for amputees are limited, for upper extremity amputee that includes hand transplantation surgery or the use of a prosthetic limb, being the latter significantly more common. The purpose of this thesis is to contribute to the advancements of prosthetic limbs.

The objective in the field of prosthetics is to replace the lost limb with an artificial limb (prosthesis). The long-term aim is to acquire a natural control of the prosthesis, which offers simultaneous control as a healthy physical limb would do. By definition "natural" in this context is to mimic the physiological system of the lost limb [2]. That entails that the input signals for prosthetic control must be obtained from the nerves and muscles that originally meant to produce the movement. Although the muscle originally meant to produce that movement is amputated, myoelectric pattern recognition (MPR) introduces the possibility to detect distant motions at the stump level and decodes the intended motion of the phantom limb [3], [4].

Electromyography (EMG) is the recording of the electrical activity induced by muscular contractions. EMG signal is most commonly acquired via sensing electrodes placed on the surface of the skin above muscle tissue. Electrodes can be defined as either surface electrodes or implantable electrodes [2]. Surface electrodes are currently most commonly used for the control of prosthesis. Implantable electrodes are a type of electrodes that are invasive but provide more localized measurements compared to surface electrodes [2].

The work in this thesis was to compare the electromyography signals obtained by two types of implantable electrodes, intramuscular electrodes (iEMG) and epimysial electrodes (eEMG). The comparison included an evaluation of signal to noise ratio (SNR), crosstalk between adjacent muscles and MPR accuracy. This comparison aimed to determine the most optimal way to acquire EMG signals for prosthetic control.

1.1 Background

Alternative solutions to a physical hand have been implemented for over a millennium, from iron hands mainly used in battle to the state-of-the-art myoelectric prosthesis used today [5].

A significant concern in the field of prosthetics has been the attachment of the prosthesis. Attachment with socket suspension shows limitations in the form of skin ulceration, sweating, pain, difficult fitting, limited range of motion, and discomfort [6]. These limitations consequently reduce prosthetic use and decrease the quality of life of amputees.

Dr. Per-Ingvar Brånemark discovered osseointegration in the late 60's. Osseointegration can provide stable fixation of bone tissue to a titanium implant [7], and nowadays, it is a conventional solution for dental implants. Osseointegration has also been suggested as an alternative for socket suspended prosthesis, relying on the direct skeletal attachment of the prosthetic limb. The first attempt to use osseointegration was on 15 May 1990 on a transfemoral amputee [8]. Osseointegration proved to be a successful alternative solution to sockets, both regarding comfort and range of motion.

Battye *et al.* initiated the development of the state-of-the-art myoelectric prosthesis in 1955 [9], she suggested using myoelectrical signal (MES) in the stump of an amputee to operate a prosthesis. MES controlled devices require the ability to discriminate against different muscle states for various movements where MPR can detect distant motions at the stump level and decode the motion of the phantom limb.

MPR was first implemented in the 1960s by Wirta *et al.* In 1977, a microcontroller unit based MPR system was introduced [10]. MPR has since been under rapid development, partly due to an improved central processing unit of modern computers and partly due to feature extraction and classifier training. Feature extraction is commonly done in pattern recognition problems to reduce the dimensionality of the data set and to correlate the stochastic nature of MES to a movement. E.g., the widely used four-time domain Hudgin's vectors, extract the mean absolute value, zero-crossing, wavelength, and slope changes of the EMG signals [11].

Classifiers are used to learn the patterns that each movement produces in the muscle, e.g., by randomly assigning feature vectors to training, validation, and testing sets. The classifiers are trained on before seen training data and validated. The classifier performance is evaluated by how well it classifies the unseen testing set.

The MPR accuracy provides a metric for the evaluation of the performance of state-of-the-art myoelectric prosthesis that incorporates the strategies mentioned above. MPR accuracy can be evaluated in different ways, with no standardized form reported [12]. Accuracy can be evaluated for both real-time and offline performance. Offline refers to previously collected data. Real-time refers to the classifier that has "learned" the patterns but has to decode the intended movements continuously in real-time. This technology is moving from the laboratories into the daily living of amputees. There are two commercially available MPR powered prosthesis, the Complete Control (CoAPT LLC, Chicago, IL) and Sense Control (IBT LLC, Baltimore, MD).

To obtain myoelectrical signals from the muscles sensing electrodes are used. The focus of this study were implantable electrodes, and due to their invasive placement, they have to fulfill the strictest requirements on medical devices. Biocompatibility is one of the significant requirements, defined by the International Organization for Standardization (ISO) and can be further divided into passive and active biocompatibility [2]. Passive biocompatibility is associated with the tissue reaction to the shape, size, composition, and mechanical properties of the electrode materials. Active biocompatibility is associated with the position of the electrodes under dynamic stress, keeping tissue injuries to a minimum and ensure that the signals are both stable and repeatable during measurements [2], [13].

Prior comparison between surface and intramuscular electrodes has been conducted by [14]–[17]. Perry *et al.* [14] evaluated the global information of the surface electrode by creating a mathematical model with information from intramuscular percutaneous implanted electrodes. Farrell and Hargrove *et al.* [16], [17] evaluated the performance accuracy of the two recording methods, which yielded little to no difference in pattern classification accuracy.

Smith *et al.* [15] in 2013 evaluated the MPR accuracy with simultaneous movements, that yielded a better result when using the signals from the intramuscular electrodes with three parallel linear discriminant analysis (LDA) classifiers.

Limited research was found for a prior comparison of epimysial and intramuscular electrodes. In 1994, Memberg *et al.* compared epimysial and intramuscular electrodes in vitro and a cat [18]. Sando *et al.* compared both epimysial and intramuscular electrodes in rats where they concluded that epimysial electrodes outperform the intramuscular hook electrodes [19].

To the best of the author's knowledge, the only article that used human subjects with a comparison between the electrodes of interests was conducted by Memberg *et al.* in 2014 [20]. There they assessed implanted myoelectric sensors (IM-MES) which is a type of intramuscular electrode with wireless communication. They concluded that the IM-MES is an acceptable alternative to the epimysial MES electrode for use in human applications.

Combining these advancements in prosthetics, Dr. Ortiz-Catalan *et al.* [21] introduced the osseointegrated human-machine gateway for long-term sensory feedback and motor control of artificial limbs, by using the osseointegrated titanium implant in combination with implanted electrodes on nerves and muscles. The percutaneous titanium component serves both as an anchor for the prosthetic limb as well as a gateway for the leads of the implanted electrodes. Such technology addresses the major limitations of current prosthetics - the lack of reliable, long-term source for control as well as the discomfort of the socket's attachment.

Significant advancements have been achieved in the field of prosthetics which motivates the need for further research to improve the functionality and reliability of prosthetic limbs [22]. Therefore, a closer look needs to be taken at the input signals used for prosthetic control. For improved prosthetic control, it has been suggested that either the use of signal processing or acquiring superior raw signals - to supply more informative input signals to the controller [17]. The latter will be explored further in this study, which type of electrode provides the most informative signals for prosthetic use.

1.2 Aim of the study

The objective of this thesis was to determine which type of muscular electrode provides superior EMG signals for prosthetic control. A framework for evaluation of intramuscular and epimysial electrodes with regards to signal to noise ratio (SNR), crosstalk, and MPR accuracy was developed and evaluated. The long-term aim of this study is to improve the quality of life of subjects with limb amputation by providing more precise and reliable control of their limb prostheses.

1.3 Ethical Aspects

Ethical approval was granted by the regional ethical committee (761-18) to perform this experiment in six subjects. The work presents the initial evaluation in one subject were both types of muscular electrodes were implanted. The volunteer provided written informed consent prior enrolment.

1.4 Thesis outline

The scope of this thesis is in five parts, listed below.

- **Chapter 1 - Introduction**
  I. Introduction to the need and thus, the motivation for this thesis.
  II. A summary of the development in the field of prosthetics.
  III. Literature review and related research of implanted electrodes.
- **Chapter 2 - Theory**
  I. Introduces general knowledge on the core concept of this thesis and thus provides a deeper understanding of the methods used.
  II. Muscles introduced in more detail and their role in EMG recordings.
  III. Electrodes and the analog front end (AFE) that interfaces the analog input signal from the electrodes to the computer.
  IV. Introduces the computations to evaluate the iEMG and eEMG signals and the software BioPatRec that acquired the signals for the comparison.
- **Chapter 3 - Methodology**
  I. The framework for the EMG recordings, from both the surgical perspective and the recording perspective.
  II. The implementation of the comparison of the electrodes with the acquired signals.

- **Chapter 4 - Results**
  I. The results from the post-processed data displayed.
  II. Impedance analysis
  III. Amplitude analysis
  IV. Crosstalk analysis
  V. MPR accuracy
- **Chapter 5 - Discussion**
  I. The discussion on the findings from the result chapter and the obstacles that presented themselves with suggestions on future improvements.
  II. Evaluation of the results and comparison of the electrodes.
- **Chapter 6 - Conclusion**
  I. The conclusion made from the single case study for the evaluation of the iEMG and eEMG signals.

2 Theory

This chapter introduces the general concepts behind EMG recordings. EMG is the recordings of myoelectric signals generated due to a muscle contraction where these recordings are widely used as a method of measuring the neuromuscular activity and selectivity of muscle activity in the body. This chapter provides an overview of how to obtain EMG signals and the information they carry. It also explains how these signals are acquired and stored. The chapter concludes by introducing the parameters used to evaluate the performance of acquired EMG signals.

2.1 Muscles

In the human body, there are three types of muscles: skeletal, smooth, and cardiac. The skeletal muscle is the only muscle type that can be voluntarily contracted [23]. Thus, it is of primary interest in acquiring information about voluntary muscle contractions.

A skeletal muscle is made up of many motor units, where each motor unit consists of a motor neuron and the group of muscle fibers it innervates [24]. Motor unit action potential is the process where the nerve transmits the signal coming from the Central Nervous System and delivers it to the group of innervated muscle fibers. This process triggers the fibers contraction, which, at the same time, generates a voltage change across the muscle tissue [25]. The recording of these voltage changes most often display the combination of multiple motor unit action potentials resulting in the known EMG waveform (an example of raw EMG signal in Figure 1).

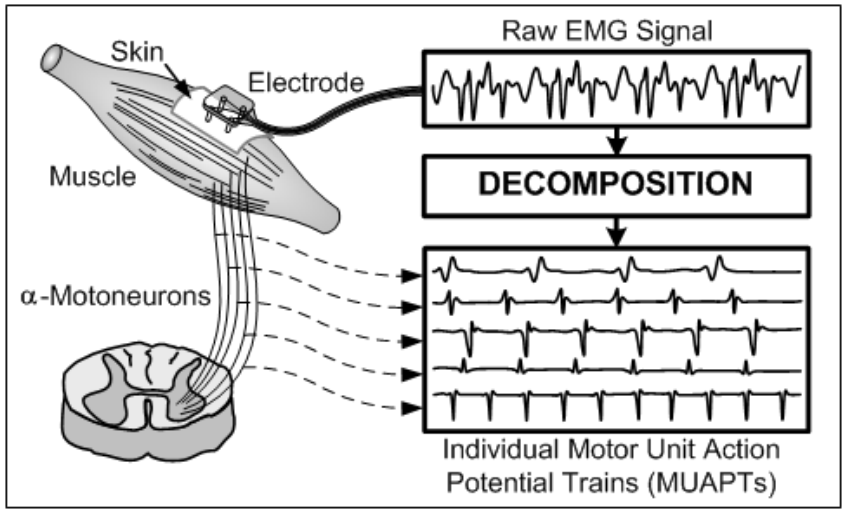

Figure 1 Displays an overview of how EMG signals are composed of multiple motor unit action potentials. Where the motoneurons deliver the signals to the muscle fibers that generate the voltage change that facilitates muscle contraction, the surface electrode placed above the muscle tissue acquires the raw EMG signals composed of all the motoneurons attached to the muscle, by decomposition individual MUAPs can be obtained [26].

Thus, the voluntarily contracted skeletal muscles produce the EMG signals that the recordings acquire. A particular focus was on the muscles located in the human forearm, due to the interest in upper limb amputees and the accessibility of the muscles in the forearm. The muscles located in the forearm can be classified as anterior/posterior and divided into three layers as superficial, intermediate, and deep. The muscles in the anterior compartment of the forearm are associated with the flexion of the wrist and the fingers, as well as pronation of the hand. The posterior compartment contains the antagonists' muscles, so the extensors responsible for extending the wrist and the fingers, and supinate the hand [23].

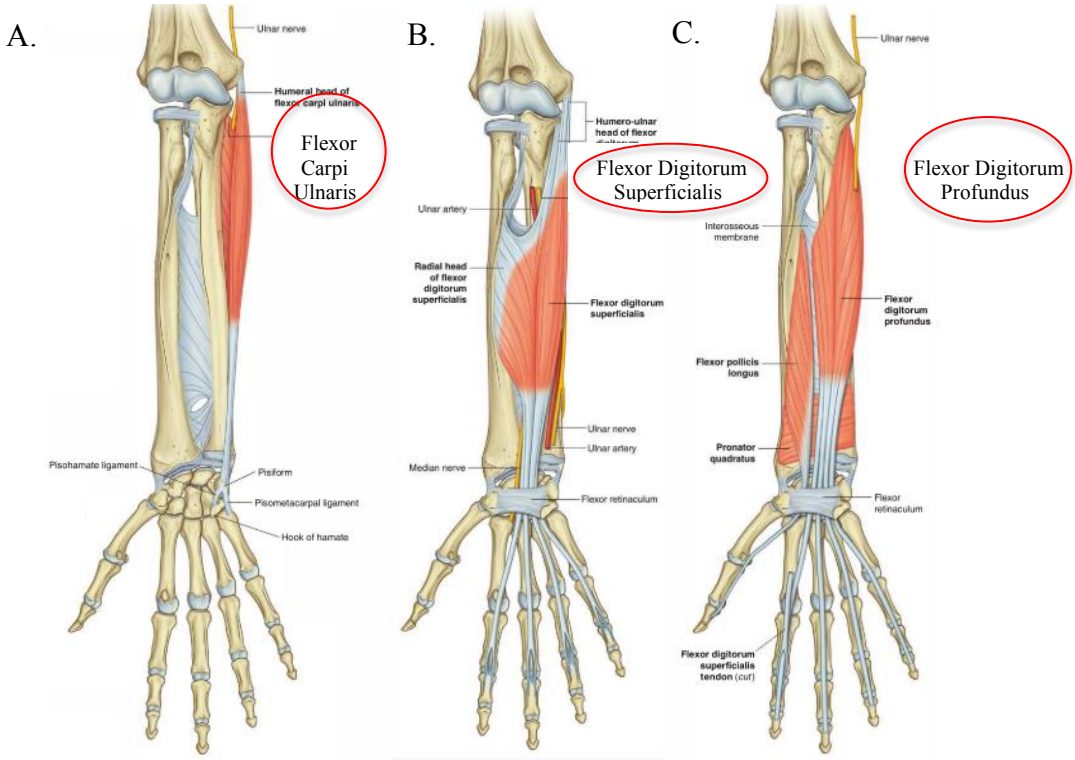

Figure 2 The anterior compartment of the forearm. A. The superficial layer of the anterior compartment highlighting the FCU muscle. B. The intermediate layer of the anterior compartment, highlighting the FDS muscle. C. The deep layer of the forearm muscle highlighting the FDP. Figure adapted from [23].

Of the twenty muscles in the forearm, three muscles associated with specific movements were chosen because of their anatomical location. These muscles are from every layer in the anterior compartment and lie adjacent to one another:

- **Flexor Carpi Ulnaris** (FCU) is one of the four muscles in the superficial layer and functions as a flexor and adductor of the wrist, i.e., ulnar deviation.
- **Flexor Digitorum Superficialis** (FDS) is the only muscle in the intermediate layer, and it acts as a flexor of the fingers. Four tendons pass through the wrist to each of the medial fingers.

The tendons attach at the joint where the metacarpals and proximal phalanges join, seen in Figure 3. The flexion of FDS results in the finger flexed from that joint [23].

- **Flexor Digitorum Profundus** (FDP) is one of three muscles in the deep layer of the anterior compartment. It passes through the wrist and into the four medial fingers. Similar to FDS but the tendons attach at both the proximal and intermediate joints of the four fingers. By contracting the distal part of the finger, i.e., the fingertip will result in selective activation of the FDP.

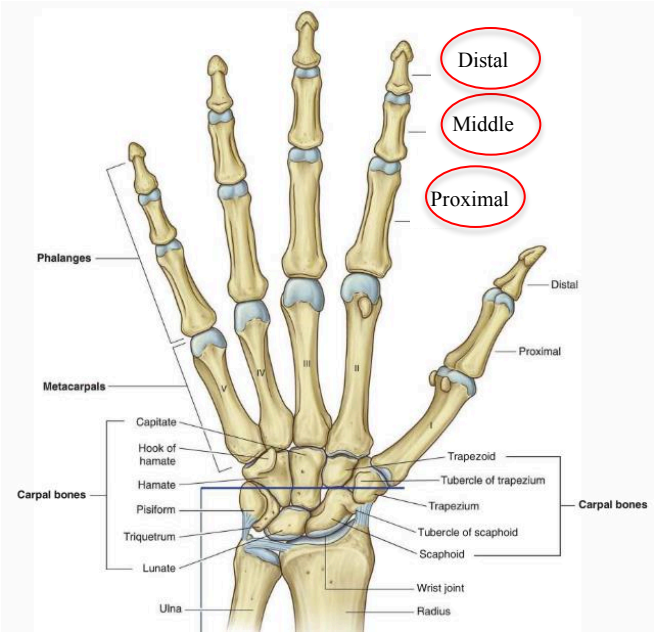

Figure 3 The hand where the distal, middle, and proximal location of the phalanges, which is highlighted in red. Figure adapted from [23].

2.2 Electrode Configuration

The EMG signals are obtained by an electrode that measures the voltage changes in the electrophysiology of the muscles. The electrode design and the recording setup configuration can vary depending on the particular requirements of the intended recording [2]. The electrode designs are most often defined as monopolar or bipolar, depending on the number of sensing plates available, one or two respectively. Consistently with the electrode design used, the signal can be acquired with single-ended or differential configurations (Figure 4). In the single-ended configuration (Figure 4A), the EMG signal sensed from a monopolar electrode located on the muscle tissue is acquired in reference to another electrode located in a distal electrical neutral tissue, namely the ground electrode. Multiple single-ended measurements (and monopolar electrodes) can refer to the same common ground electrode.

In the differential configuration (Figure 4B), the EMG signal is instead acquired from two electrodes, often spatially close to each other within a bipolar design. The acquired signals, either referred to the same ground or "non-grounded", are then subtracted to obtain the differential measurement [24].

For a bipolar electrode design acquired with a differential configuration, the inter-electrode distance can greatly impact the amplitude of the acquired signal. In fact, the closer the inter-electrode distance, the smaller the output and the crosstalk from neighboring muscles [24], [27].

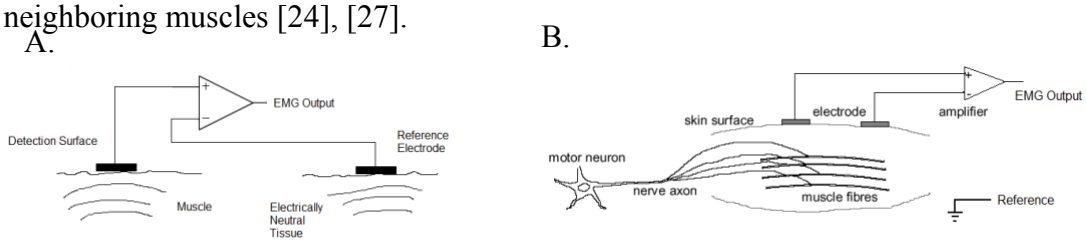

Figure 4 The two different electrode configurations [25]. *A. The monopolar configuration where positive input to the amplifier placed on the muscle tissue and the negative input placed in an electrical neutral tissue. B. The bipolar configuration shows how both inputs to the amplifier placed on top of the muscle tissue with a small inter-electrode distance. - the reference electrode placed in electrical neutral tissue.*

There are trade-offs between both configurations. The monopolar configuration yields a higher amplitude of the EMG since it compares the signal to a reference at zero voltage and requires one lead for the signal acquisition and one for the reference. The bipolar configuration shows the differential voltage between two electrode contacts and displays their potential difference. Consequently, there is less crosstalk, but smaller signals, and it requires two leads with additional reference lead [17], [24].

2.3 Electrodes

There are several types of biopotential electrodes used for acquiring EMG signals. The electrodes used for prosthetic applications can be divided into two categories. The first category includes surface electrodes, which are non-invasive and located over the skin. Surface electrodes have been most widely used in myoelectric prosthetic control to this day [2]. The second category includes implantable electrodes. These are invasive solutions that can provide more localized recordings than surface electrodes. The implanted electrodes are further classified into muscle-based electrodes and nerve-based electrodes. The scope of this thesis is limited to the evaluation of two types of implanted muscle-based electrodes.

The two types of muscle-based electrodes of interest for this study are intramuscular and epimysial. These are differentiated by the location of implantation, either inside the muscle or outside the muscle on the epimysium.

Intramuscular electrodes are placed inside the muscle using guiding fine-needle. EMG recordings acquired by intramuscular electrodes shall be referred to as iEMG recordings for the remainder of this thesis. iEMG is known to provide localized measurements of the activation inside of the muscle [24].

Epimysium is the tissue envelope that surrounds skeletal muscle. Epimysial electrodes are sometimes called extra-muscular electrodes since the placement is outside the muscle. Surgery is required to attach the electrode to the epimysium. These electrodes are sown on the epimysium that surrounds the muscle. EMG recordings acquired by epimysial electrodes shall be referred to as eEMG recordings.

2.4 Analog Front End

Signal acquisition hardware must provide the source signals for further processing. The electrodes acquire the analog EMG signals from the muscle activation. Converting the EMG from analog to digital form requires discretization, i.e., the process of transferring continuous variables into its discrete counterparts. That transformed number then stored in a binary format for the MCU for post-processing. The sampling rate and the number of bits determine the quantity and speed of digitization.

Analog Front Ends (AFEs) interface the analog input of the EMG signals to the digital MCU. Signal acquisition hardware for EMG signals is aimed to record low amplitude signals. In addition to acquiring the signals, the AFEs are often designed to amplify, bandpass filter, and condition the signals before sending the signals to the analog-to-digital converter (ADC). AFEs that are compact and low noise are rising in importance for the bioelectric signal acquisition of a portable system [28].

2.5 BioPatRec

The open-source modular platform BioPatRec in MATLAB (MathWorks, USA), acquires EMG signals for prosthetic control and has multiple functions for signal processing [29]. An overview of the functionality of the software seen in Figure 5.

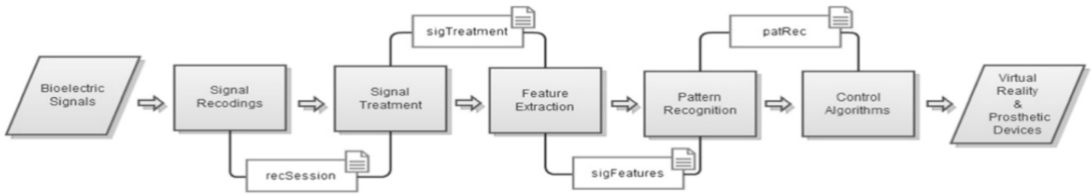

Figure 5 Displays an overview of the different modules available in BioPatRec and the Figure was obtained from [29]. *The Signal Recording module acquires the EMG signals and displays guided movements in a dedicated GUI. The Signal Treatment module is used to reduce the dimensionality of the data from the Signal Recording, by the use of taking a central percentage of the contraction period and by dividing the signals into overlapping windows. Feature Extraction module performs discretized characterization of the signals and, the Pattern Recognition module performs the offline classification of the signals with various options of classifiers. The Control Algorithms module has two options for evaluating real-time performances. The Motion Test and the Target Achievement Test (TAC) test* [30], [31].

2.6 Computations

2.6.1 Impedance

For implanted conductive electrodes, the primary requirement is to establish a low impedance contact with the tissue and the implanted electrode. To evaluate the impedance of an implanted electrode, the electrode-tissue interface is approximated to an electric circuit. Ohm's law derives the voltage (V) given that direct current (i), and resistance (R) is known. Resistance found if the voltage and current are known as seen in Equation 2.1. Equation 2.2 shows the Ohm's law rewritten for an electric circuit supplied with alternating current (AC).

$$V = i * R \Rightarrow R = \frac{V}{i} \qquad \textit{Equation 2.1}$$

$$V = i * Z \qquad \textit{Equation 2.2}$$

The body can be modeled as a capacitor and a resistor, and the capacitive behavior can be observed when the electrodes are supplied by alternating current. AC supplied circuit has a combined effect of complex ohmic resistance (X) and reactance (jR). Equation 2.3 shows that the impedance (Z) is comprised of the magnitude (real component vector) and the phase (imaginary component vector).

$$Z = X * jR \qquad \textit{Equation 2.3}$$

The impedance Z is extracted by approximating the body to an electric circuit.

2.6.2 Root Mean Square (RMS)

For a sample of signals,
Equation 2.4 as the name indicates takes the root mean square (RMS) over an integral of signals. Used to normalize the contraction period of the maximum voluntary contraction (MVC), due to the stochastic nature of the EMG signals.

$$x_{RMS} = \sqrt{\frac{1}{N} * (\mathrm{x}_1^2 + \mathrm{x}_2^2 + \cdots + \mathrm{x}_\mathrm{n}^2)} \qquad \textit{Equation 2.4}$$

2.6.3 Signal to Noise ratio (SNR)

Mastinu *et al.* evaluated the SNR as the ratio of signal amplitude to noise amplitude of the obtained EMG in the time domain [28]. The signal (S) defined as integral over the RMS value of the signals' recorded during a muscle contraction, and noise (N) is the integral over the RMS value of the baseline of the signal when the muscle is at rest. The SNR often displayed on a logarithmic decibel scale due to the broad dynamic range of the signals, shown in Equation 2.5.

$$\mathrm{SNR}_{\mathrm{dB}} = 10 * \log_{10} \frac{S_{RMS}^2}{N_{RMS}^2} \qquad \textit{Equation 2.5}$$

2.6.4 Cross-Correlation

To quantify the amount of crosstalk, i.e., the signals that are generated from the adjacent muscles and influence the targeted muscle was evaluated between neighboring muscles. The most common approach to quantify crosstalk is the cross-correlation function [32]. Traditionally, crosstalk has been measured by evaluating the peak value of cross-correlation between a pair of electrodes. Key features are peak correlation value, value at a zero-phase shift, and the timing of zero-crossings.

Equation 2.6 shows the two signals x(t), and y(t) and T is the length of the signals being cross-correlated. The signal y(t) shifts by τ over the signal x(t), computing the correlation at each time interval. The higher the result from the equation, the higher the correlation is between the two signals. A higher correlation indicates crosstalk between the compared signals.

$$R_{xy}(\tau) = \frac{1}{T}\int_0^T x(t)y(t+\tau)dt$$

Equation 2.6

There are problems related to Equation 2.6, where the value is hard to interpret. Problems with detecting correlation with a varying amplitude of signals and zero values are not taken into account since it is a multiplication with 0. Normalized cross-correlation solves these problems, the normalized form of the cross-correlation function where the results lie between -1 and 1 seen in Equation 2.7.

$$R'_{xy}(\tau) = \frac{R_{xy}(\tau)}{\sqrt{R_{xx}(0)R_{yy}(0)}}$$

Equation 2.7

$R_{xx}(0)$ is the autocorrelation of the signal x(t) at the time shift $\tau = 0$. The same goes for $R_{yy}(0)$ for the signal y(t). Autocorrelation is applicable for detecting repeatable patterns of signals.

2.6.5 Myoelectric Pattern Recognition (MPR)

Myoelectric pattern recognition (MPR) decodes the intended motion and can be developed to achieve more intuitive control, based on specific EMG patterns recorded from the residual limb of amputees. For evaluating the performance of the MPR algorithm, the classification accuracy is the most common way [12].

There are different ways to evaluate accuracy with no standardized from, the global accuracy is the most general and is shown in Equation 2.8 [12]. The acronyms stand for true positive (TP), true negative, (TN), false positive (FP) and false negative (FN). The definitions of these acronyms where TP is a correct activation, TN is a correct inactivation, FP is a false activation, and FN is a false inactivation. The global accuracy is a percentage of times that the correct classification manages to decipher the intended movement of the subject. The classification accuracy can be influenced by the window length, extracted EMG signal features, type of classifier, and the division into training, validation, and testing sets [33].

The class-specific accuracy (CS accuracy) considers the outcome of each movement class individually and is preferred in multi-class evaluations to dismiss false outcomes for any movement [12]. The BioPatRec approach to evaluate MPR accuracy shown in Equation 2.8 [34]. The CS accuracy evaluated with correct classifications divided by the total number of true and false classifications.

$$Global\ Accuracy = \frac{\sum TP + \sum TN}{\sum TP + \sum TN + \sum FP + \sum FN} \qquad \textit{Equation 2.8}$$

$$CS\ Accuracy = \frac{absolotue\ correct\ predictions}{total\ absolute\ predicitons} \qquad \textit{Equation 2.9}$$

3 Methodology

This chapter describes the methodology used in the study to draw a comparison between EMG signals recorded from epimysial and intramuscular electrodes placed in an able-bodied volunteer. The first part of the chapter describes the methods followed to surgically implant the electrodes in the volunteer enrolled in the study. The second part of the chapter describes the methods followed to acquire, process, and compare the EMG signal recorded from both epimysial (eEMG) and intramuscular (iEMG) electrodes.

3.1 Procedures for Surgical Implantation

Ardiem Medical, Inc. fabricated and manufactured the electrodes used in this study. The electrodes were supplied sterile and in sterilized packaging. Both electrode types were designed for Integrum AB, schematics, shown in Figure 7.

The percutaneous leads of the intramuscular electrode were comprised of a seven-strand type stainless steel 316 LVM wire with perfluoroalkoxy (PFA) tubing for insulation. The electrode body was in silicone with exposed bipolar contacts. A polypropylene anchor attached at the distal end ensured the mechanical stability of the electrode.

The epimysial electrode percutaneous leads were comprised of a Drawn Filled Tubing (DFT) wire and PFA insulation. The electrode body was in silicone with exposed bipolar contacts, 90% platinum, and 10% iridium (PT90/IR10). The silicone body was sutured on the outer layer of the muscle to ensure mechanical stability.

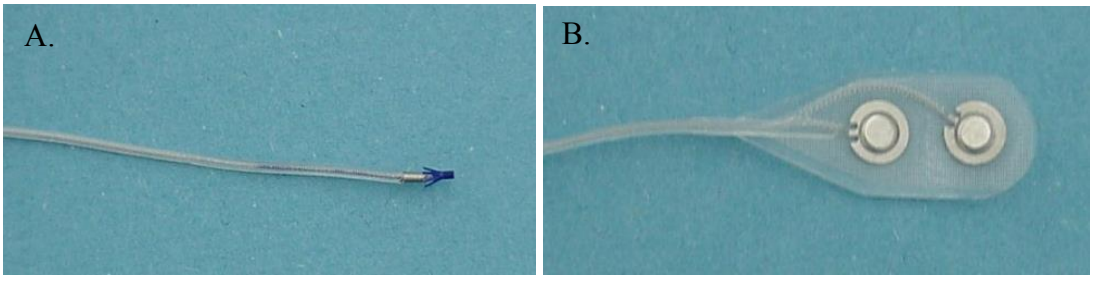

Figure 6 The two types of implanted muscle-based electrodes used to conduct this study. A. The intramuscular electrode B. The epimysial electrode.

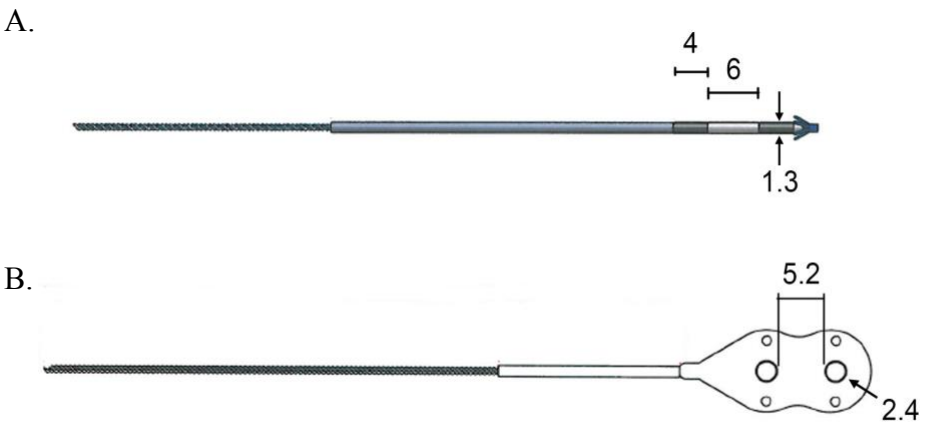

Figure 7 The schematics of the implanted electrodes with relevant dimensions for this study. A. The intramuscular electrode, with IED as 6mm, the length of each contact was 4 mm and the diameter 1.3 mm. B. The epimysial electrode, where the diameter exposed contact area was 2.4 mm and the IED 5.2 mm.

3.2 Implantation

The implantation was performed by a hand surgeon at the Hand Surgery Department of the Sahlgrenska Hospital in June 2019. One able-bodied volunteer participated in this study (age 26 years) for sixteen days. The ethical approval (Dnr: 761-18) was obtained from the Swedish regional ethical committee in Gothenburg. Written informed consent was given prior to any data and media collection.

3.2.1 Electrode Placement

The selection of the muscle targeted in this study was critical. The requirements were:

- Accessibility for implantation
- Nondominant muscle
- Positioned adjacent to large muscles

The limitation of tissue trauma for the volunteer was considered a priority. The location of the electrodes was chosen to minimize the mechanical stress and strains. This was necessary to avoid damage to the tissue or to the electrodes. Moreover, this allowed more repeatable recordings from a localized site.

Flexor Carpi Ulnaris (FCU) was found to fulfill the requirements for the EMG recordings while not overcomplicating the surgical procedure. The location of the FCU is in the superficial layer of the anterior compartment of the forearm. Its main functionality is the flexion and ulnar deviation of the wrist [23].

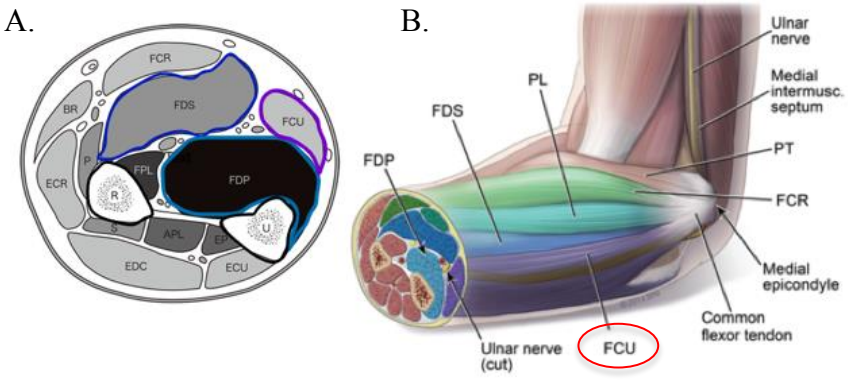

Figure 8 Schematics to visualize the muscle anatomy of the forearm A. Displays the circumference of the forearm with highlighted muscles of interest. The muscle FCU and its vicinity to both FDS and FD, adapted from [35] *B. Shows the anatomical location where the highlighted FCU was implanted approximately 5cm from the elbow adapted from* [36]

By activating the FCU and using palpation, the exact location of the muscle was determined. Under local anesthesia, a 2,5cm incision over the FCU was made to insert the electrodes, and another 1,5cm incision more distal from the elbow was made to thread the connector out percutaneously. The double incision was preferred to minimize the risk of infection to the electrode site.

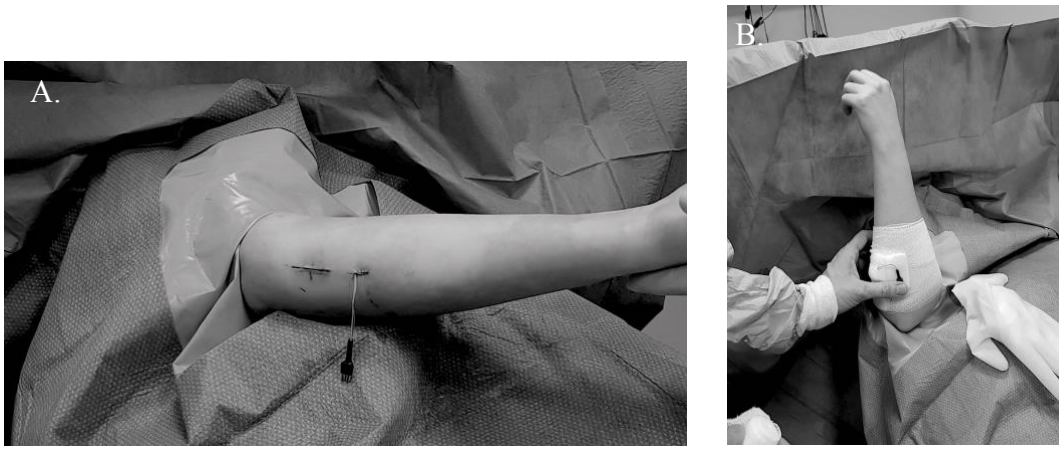

Figure 9 The surgical implantation of the electrodes and the percutaneous placement of the connector. A) Displays how the incisions were made, where the proximal incision to the body is where the electrodes were placed, and the distal incision is where the connector penetrated the skin. The two incisions were made to reduce the risk of infection to the electrode site. B) Shows how the incisions were covered and how the connector was placed.

Crosstalk was induced by performing selective movements to activate the adjacent muscles. The movements facilitated the activation of the targeted muscle FCU and the adjacent muscles FDS and FDP. As Table 1 reveals, there are many muscles associated with these selective movements and the highlighted marks show the most selective activation of the muscles of interest.

Table 1 Simplified muscles-movements relation considered in this study.

Movements	FCU	FDS	FDP	FCR	FPL	ECU	ECR	EDC
Open Hand								x
Close Hand		x	x		x			
Flex Wrist	x	x		x				
Extend Wrist						x	x	x
Ulnar Deviation	x							
Radial Deviation				x		x	x	
Index Finger Flexion		x						
Middle Finger Flexion		x						
Ring Finger Flexion		x						
Flexion of Distal Phalanges			x		x			

Abbreviations: FCU: Flexor Carpi Ulnaris, FDS: Flexor Digitorum Superficialis, FDP: Flexor Digitorum Profundus, FCR: Flexor Carpi Radialis, FPL: Flexor Pollicis Longus, ECU: Extensor Carpi Ulnaris, ECR: Extensor Carpi Radialis longus/brevis, EDC: Extensor Digitorum Communis

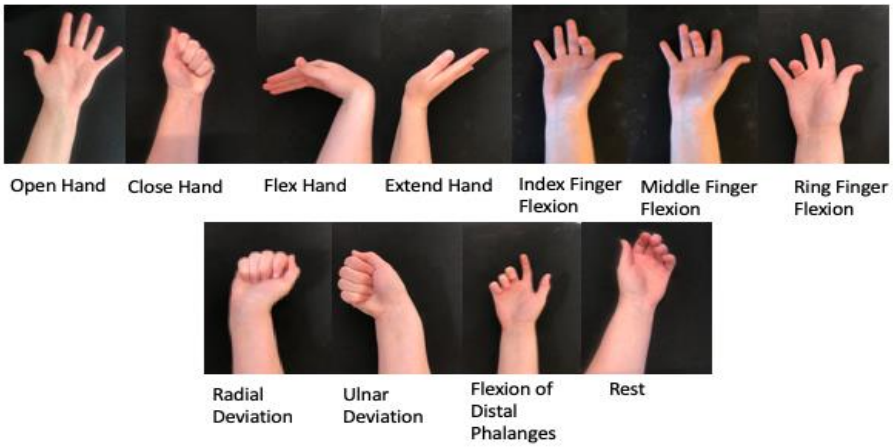

Figure 10 The ten movement classes and rest. These movements were selected to target specific muscle activations for the recording sessions.

3.3 Measurement Procedure

3.3.1 Analog Front End Systems

Three different AFEs were used for signal acquisition. This was deemed appropriate in order to obtain different characteristics of the EMG signals, to compare acquisition topologies (e.g., monopolar vs. bipolar), and ultimately to provide a wider perspective for the comparison of the electrodes.

Table 2 displays the main characteristics of the AFEs used in the study. The comparison between the acquired EMG signals and individual systems took into account the different characteristics of each AFE.

Table 2 Configuration of each analog front-end system. Regarding amplifier topology, the acquisition chip used, the bandwidth to acquire the signals, amplification, and the digitalization of the signals. Note, the gain for MyoAmpF4F5 is variable from 50-5000.

Device	**Amplifier topology**	**Acquisition chip**	**Band-Pass [Hz]**	**Gain**	**Digitalization**
Artificial Limb Controller [37]	Monopolar	RHS2116 (Intan Technologies, USA) [38]	20-500	192	1kHz & 16 bits
ADS_BP [39]	Bipolar	ADS1299 (Texas Instruments, USA) [40]	20-524	24	2kHz & 24 bits
MyoAmpF4F5	Bipolar	DAQ Device NI USB-6212 (National Instruments, USA) [41]	20-1000	~500	5kHz & 12 bits

The Cannon 2D/CTA series pin and socket connector (ITT Cannon, CA, USA) was used to connect the electrodes to each of the AFEs. Figure 11 shows a simplified version of each amplifier configuration to visualize the acquisition topologies for the different devices used.

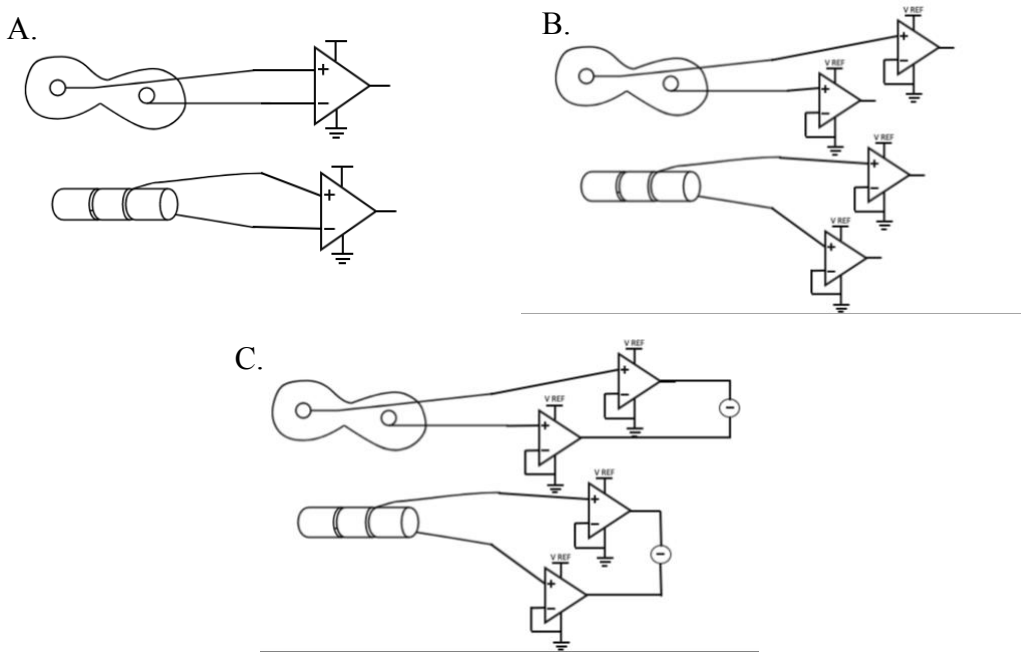

Figure 11 The different amplifier topologies. A. Bipolar configuration. B. Monopolar configuration. C. Software bipolar configuration, where the monopolar channels for corresponding electrode are subtracted with each other, to be comparable with the signals obtained by the bipolar configuration.

3.4 Recording Sessions

The signal from both iEMG and eEMG channels were acquired simultaneously. The volunteer had the electrodes implanted for roughly two weeks, where a total of three recording sessions were performed. Each recording session took approximately 1½ - 2 hours. Three different AFEs were used to acquire the EMG signal, interfaced via the PC software BioPatRec [42]. A set of protocols were followed for every session and available in a separate document in details.

Table 3 The date of each recording session performance and the days post-implantation. Date of implantation (DOI), date of ex-plantation (DOE)

	Recordings performed				
	DOI	**Session #1**	**Session #2**	**Session #3**	**DOE**
	24.06.2019	28.06.2019	01.07.2019	04.07.2019	10.07.2019
Days post-op	-	4 days	7 days	10 days	16 days

Table 4 Shows the schedule of which recordings were performed for each system during every session. The different recordings and computations were done to gather as much information as possible over the short period of the study.

AFE	ADS_BP			ALC			MyoAmpF4F5		
	Sessions								
Recording Session #	**#1**	**#2**	**#3**	**#1**	**#2**	**#3**	**#1**	**#2**	**#3**
MVC Recording	x	x	x	x	x	x	x	x	x
Ramp Recording		x			x			x	
PatRec Recording	x	x	x	x		x	x		x
Offline MPR	x	x	x	x	x	x	x	x	x
Real-time MPR	x	x	x		x				

3.4.1 Impedance

Every recording session started with a measurement of the impedance of the electrode's contacts. The impedance was measured both manually and automatically. The manual measurement was performed by stimulating the electrodes with a single rectangular electric pulse with the amplitude of 150μA and width of 100μs. The consequent voltage was displayed on an oscilloscope. The 1voltage differed from the perfectly rectangular shape provided as input, showing a charging rise profile typical of capacitive load. The rise and the peak values were of interest. The peak of the output voltage was measured from the oscilloscope and used to compute the resistance magnitude via Ohm's law. Moreover, automatic impedance measurements were performed via a graphical user interface (GUI) in MATLAB (MathWorks, USA) designed for the ALC [37]. Thus, two sinusoidal stimulation waves were delivered to each electrode type contacts for separate impedance measurements while the generated voltage was measured automatically after. The two sinusoids were delivered at two different frequencies allowing for an estimate of both the imaginary and the real part of the contact impedance. An automatic measurement took around 30 seconds per contact. The manual and the automatic impedance measurements were compared to provide better insight.

3.4.2 Recording Session for Amplitude Comparison

The participant sat in front of a computer where the recording software was installed (BioPatRec and MATLAB R2019a). All movements were clarified and practiced during the first recordings session.

Ten movement classes were recorded in a randomized order: open/close hand, wrist flexion/extension, ulnar/radial deviation of the wrist, index/middle/ring finger flexion and flexion of distal phalanges of index/middle/ring fingers. Instruction on a GUI showed the intended movements for the participant as well as the time duration for both contraction and rest. Two different recording types were performed for the scope of the amplitude comparison, namely MVC and ramp recordings.

The MVC recording collected 3 seconds of MVC for each ten movement classes. Here, the subject was instructed to provide 100% of their contraction force while correctly performing the movement. The randomized movements were displayed in a GUI with a 3-second countdown between each contraction. These recordings were executed for each recording session for every system, either as a separate recording or from the ramp tracking recording.

Ramp tracking recording was performed only once per AFE system. Each ramp recording started with collecting 3 seconds of minimum voluntary contraction (e.g., rest state). Consecutively, 3 seconds of MVC was performed for all movements similarly to the MVC recording aforementioned. The rest state and the MVC values were used to provide a reference for the next part, the ramp tracking. The reference was required to calculate and display a real-time visual feedback of the amount of muscular effort delivered by the subject. This feedback was then used to allow the subject to perform the movements with constantly increasing muscular effort represented by a guiding ramp, where the average effort increases in proportion between the rest state and MVC previously recorded. During the ramp tracking recording the GUI continuously updated the muscular effort visual feedback. The subject was instructed to perform the movements with a muscular effort that stayed on or above the guiding ramp displayed in the GUI. Each movement was repeated three times, alternating 3 seconds of contraction with 3 seconds of relaxation. By slowly increasing the contraction force, these recordings can provide insight for proportional control and the summation of action potential as muscle contraction increases.

3.4.3 Recording Session for Pattern Recognition Comparison

A different type of recording, namely PatRec recording, was performed for the pattern recognition comparison. That entailed to executing all the movement classes, in randomized order, with a comfortable contraction force (around 60%).

Each movement was repeated three times, alternating 3 seconds of contraction with 3 seconds of relaxation.

3.5 The comparison: eEMG vs iEMG

The signals acquired from every recording session were used for the comparison of eEMG and iEMG signals.

Table 5 An overview of which computation was performed from which recording method. Note that the ramp recording was not used for obtaining the conclusion for this thesis.

Calculations	Recordings	
	MVC	**PatRec**
RMS	x	
SNR electrodes per device		x
SNR mono vs. bi-polar	x	x
Cross-correlation		x
Offline MPR		x
Real-time MPR		x

3.5.1 EMG Amplitude

3.5.1.1 Root Mean Square

The RMS values were computed from the MVC recordings of each electrode and for individual movement (Equation 2.1), with MVC recording from every session for each separate AFE. The main interest was to see the difference between monopolar and bipolar acquired signals. Additionally, we calculated the software-differential measurements from the two poles for each electrode that the monopolar system, ALC acquired. For this reason, the monopolar measurements between the paired couples of contacts were subtracted (Figure 11C).

3.5.1.2 Signal to Noise Ratio

SNR is a statistical ratio that indicates the quality of the EMG signal by dividing the signal S with the noise N as in Equation 2.5. These vectors of S and N data were acquired in the previously mentioned recording sessions.

For electrode type comparison for individual system, the PatRec recordings were used. To exclude the majority of artifacts and still contain the most relevant information, the signals were trimmed to 70% of the central contraction period. An identical process performed to extract 70% of the central rest state in-between contraction windows. The vectors were then concatenated in two different arrays, signal S and noise N respectively.

The RMS was computed for all the extracted data for each movement. Both arrays were squared, and the SNR was computed by substituting them in Equation 2.5. It is displayed on a logarithmic decibel scale due to the broad dynamic range of the signals and performed for each electrode for every movement for each system.

To compare SNR between individual devices the values obtained from the MVC recordings were used. From the 3000 samples acquired for the repetition of each movement, the central 2000 samples were extracted and used with the central 2000 samples from the resting-state.

Additional SNR calculation was performed to see the effect of crosstalk from a different perspective. Similar to the SNR described above with the main difference in a different classification of the noise vector N. The signal vector S was obtained from the targeted muscle while performing the ulnar deviation movement. The corresponding noise vector N for the SNR formula was not only the baseline as above but also the activation of the adjacent muscles, FDP and FDS as well as the antagonistic muscle ECU. These specified movements were used as input in Equation 2.5 - again to perform SNR calculations with the differently classified S and N's.

3.5.2 Crosstalk

To quantify the crosstalk between neighboring muscles the cross-correlation function shown, in Equation 2.6, was used. This equation has been most commonly used to quantify crosstalk with surface electrodes [32]. The cross-correlation function correlates two signal sequences together by shifting the placement relative to the other and thus can indicate the similarity between the two. For this study, the activation of the targeted muscle was used and cross-correlated to the "noisy" movements, mainly the ones activating the adjacent muscles and the antagonistic muscle. A higher correlation value indicates increased crosstalk between the compared signals.

3.5.3 Pattern Recognition Evaluation

The offline and real-time MPR evaluation was performed using the modules available on BioPatRec software.

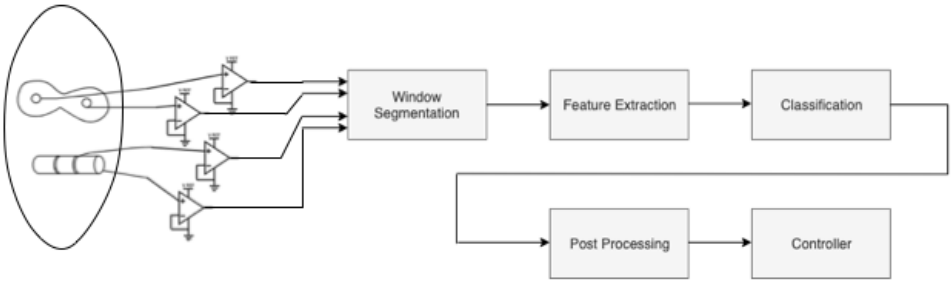

Figure 12 Schematic diagram of a typical MPR classifier, as the ALC system using the electrodes for this study, computes. Adapted from Farrell et al. [15].

3.5.3.1 Offline Pattern Recognition

The prior stored PatRec recordings were uploaded to the Pattern Recognition module of BioPatRec. The recorded EMG signals were window segmented, i.e., the signal was divided into 200ms overlapping windows with 50ms of overlap [29]. After the signal segmentation a set of features were extracted, as commonly done in pattern recognition problems to reduce the dimensionality of the data set. The feature extraction for MPR used the four-time domain Hudgin's vectors [11]. The feature vectors were then randomly assigned to 40% testing, 20% validation, and 40% training sets [21]. The LDA classifier was trained in one-vs-one (OVO) topology. The classifier training was reiterated ten times, and the average offline accuracy was calculated. The accuracy of every system was extracted and graphically presented.

Additionally, the interest was to evaluate the accuracy of each electrode separately. The signal treatment GUI provides the option to select the channels of interest to use for the MPR. Therefore, the same procedure as above was repeated for individual channels to present the difference in MPR accuracy graphically.

3.5.3.2 Real-time Pattern Recognition

The Motion Test, introduced by Kuiken *et al.* [31] and available in BioPatRec, was used for the real-time evaluation of the pattern recognition algorithm performance.

During the Motion Test, a GUI requested the subject to perform movements. Moreover, the GUI informed the subject if a total of 20 correct classifications were obtained within the 10s timeout given to each trial. Each trial was performed with three randomized repetitions of all the movements included in the recording session. The Motion Test comparison was used to compare the accuracy, completion rate, completion time, and selection time versus each movement and each electrode recording method. The real-time accuracy for each electrode was computed to compare their performance acquired by the ADS_BP recordings.

4 Results

4.1 Impedance Analysis

The rise and the transient of the capacitive wave were documented for the manual impedance measurement. A stimulation pulse of 150µA was sent from the ALC and through the approximated modeled RC circuit of the body. The response of the stimulated pulse was visualized on an oscilloscope (Figure 13). By knowing the stimulation pulse and the voltage generated, the impedance of the circuit was obtained (Table 6).

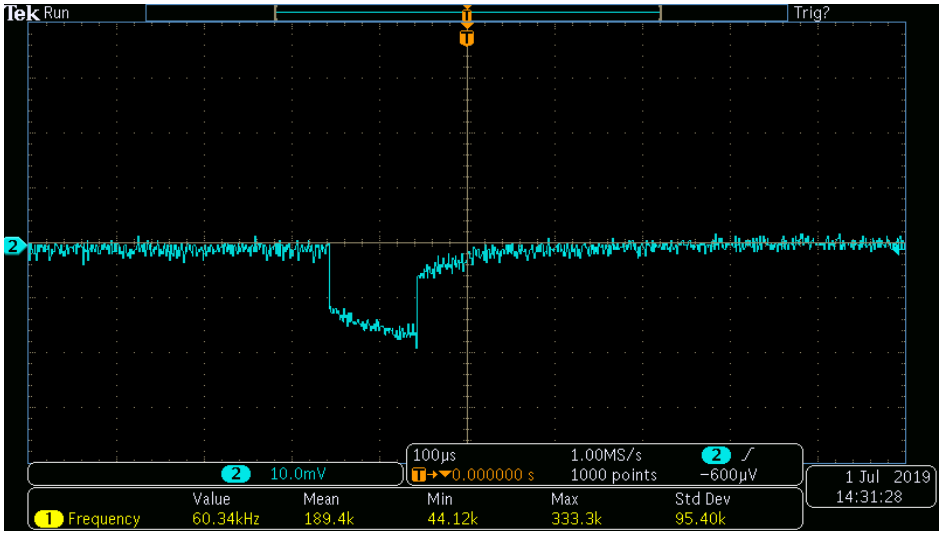

Figure 13 A screenshot from the oscilloscope during a manual impedance measurement. It displays the response of the rectangular pulse sent through the system; each box on the image represents 10mV.

Table 6 The results from the manual and automatic impedance. All values displayed in Ω. The automatic impedance values are the average from both channels associated with that circuit.

		Manual Impedance		
Days Post-op		**0 (DOI)**	**4**	**7**
IM	Rise	1467	667	800
	Transient	2200	1000	1133
EP	Rise	1200	1000	1133
	Transient	2133	1533	1333
		Automatic Impedance		
IM		1369	1274	1316
EP		1504	1110	1208

4.2 Amplitude Analysis

4.2.1 RMS Analysis

From the MVC recordings, the RMS peak values were obtained (Table 7). The peak values were compared between the electrodes for the ADS_BP and ALC systems. The amplitude of the peaks corresponds to the gain that the systems provide where each AFE had different characteristics (Table 2), and the values were not normalized.

Table 7 The peak RMS values from acquired MVC signals. All values displayed are in µV (standard deviation). The standard deviation is only applicable to the ALC measurements since one MVC recording was obtained with the ADS_BP. Note, the MVC values of the MyoAmpF4F5 were not viable for comparison.

Systems	**ADS_BP**		**ALC bipolar**	
	Recording electrodes			
Movements	**eEMG**	**iEMG**	**eEMG**	**iEMG**
Open Hand	69.76	18.31	447.27 (63.79)	416.08 (61.94)
Close hand	39.59	15.29	502.98 (111.58)	450.58 (99.60)
Flex Wrist	99.83	19.60	381.60 (100.18)	301.42 (83.07)
Extend Wrist	18.23	13.13	452.55 (52.90)	396.52 (46.23)
Ulnar Deviation	14.43	7.18	266.91 (51.70)	248.46 (53.60)
Radial Deviation	6.27	6.54	223.33 (46.72)	218.45 (46.41)
Index Finger Flexion	11.72	12.69	214.29 (41.26)	222.86 (49.60)
Middle Finger Flexion	14.26	7.89	345.07 (89.44)	333.74 (89.05)
Ring Finger Flexion	22.36	10.33	367.99 (80.04)	341.86 (75.52)
Flexion of Distal Phalanges	16.28	8.41	293.88 (110.48)	276.67 (101.03)

4.2.2 SNR Analysis

The main objective was to compare the SNR from the two types of electrodes. The SNR values for each electrode and the individual systems, ADS_BP and ALC (Figure 14).

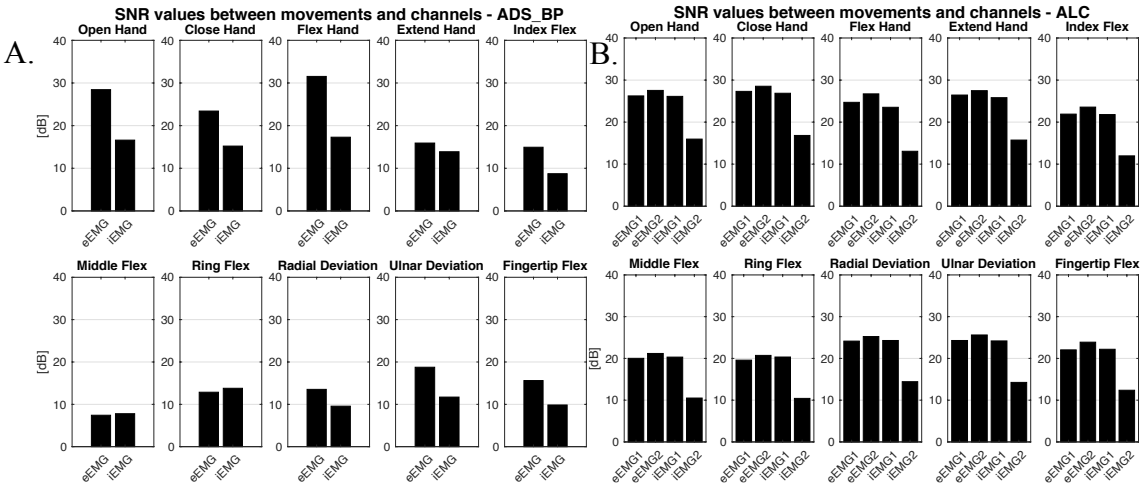

Figure 14 A. The SNR values between movements for each bipolar channel obtained by the ADS_BP system B. The SNR values between movements for each monopolar channel obtained by the ALC system.

To be able to compare the AFEs displayed in Figure 14, the software bipolar version was computed from the ALC recordings. The SNR comparison can be visualized in Figure 15.

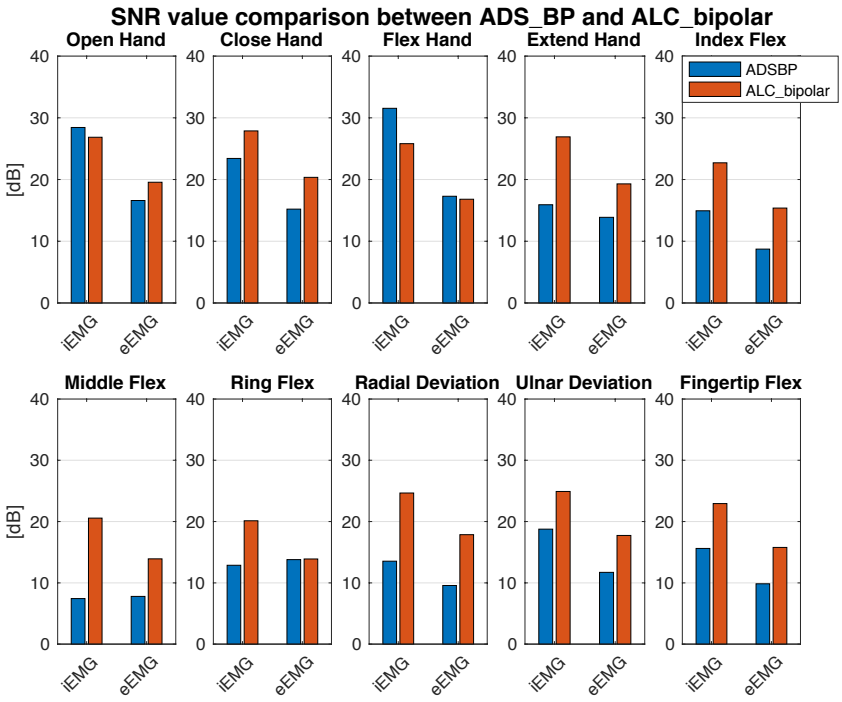

Figure 15 The SNR values compared between bipolar system for every movement, for ADS_BP and ALC.

4.3 Crosstalk

The cross-correlation function was used to correlate the targeted muscle with the signals from the adjacent muscles as well as the targets muscle antagonist. The results for those selective movements for every system are shown in Figure 16.

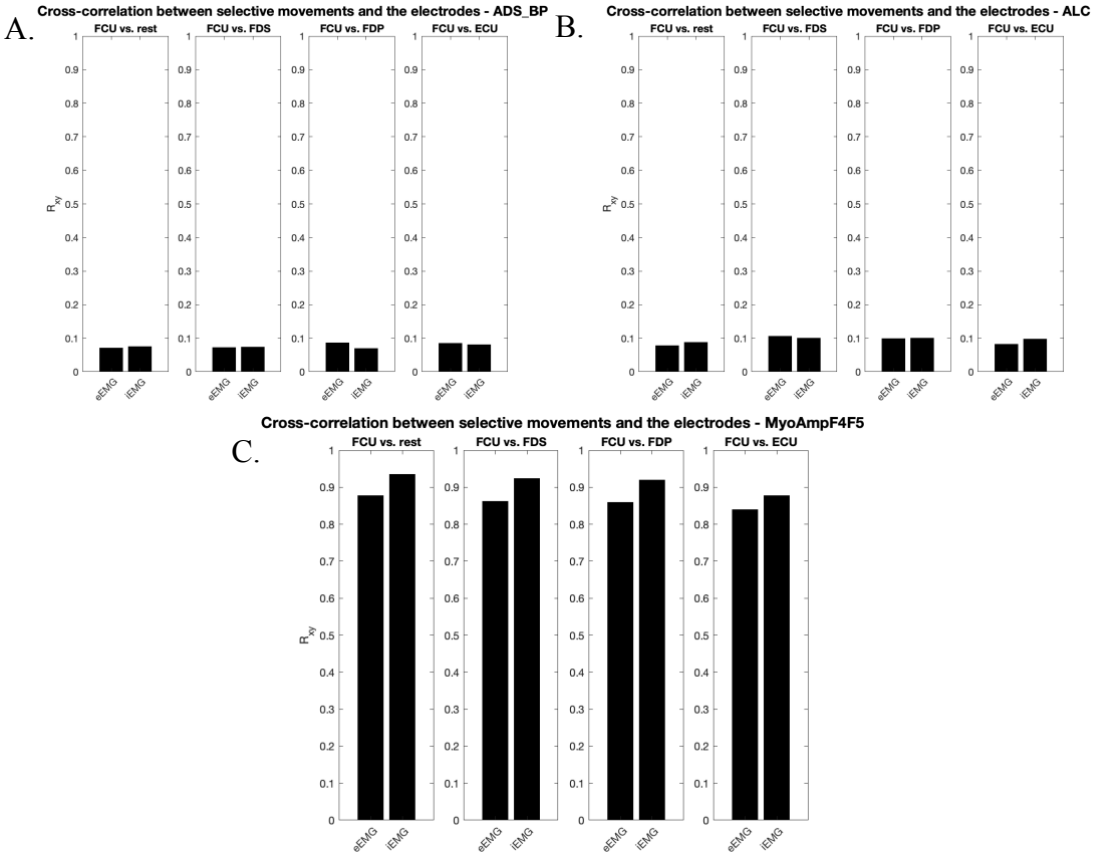

Figure 16 Cross-correlation value R_{xy} between all three systems, as can be observed. The targeted signal was compared with the adjacent muscles and the antagonist muscle. Note the significantly more crosstalk from the MyoAmpF4F5 recording compared with the ADS_BP and ALC_bipolar.

A different approach to evaluate crosstalk was through SNR analysis. The same signals as used for in the cross-correlation function, namely the activation of the targeted muscle FCU compared with rest, the activation of the adjacent muscles (FDS, FDP) as well as the activation of the antagonistic muscle (ECU) was executed. The eEMG and iEMG recordings were compared between systems for selective movements.

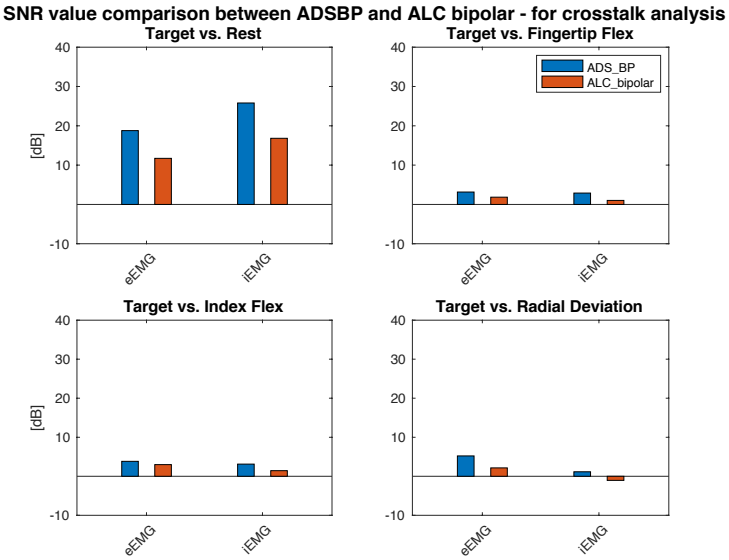

Figure 17 The SNR comparison between selected movements for ADS_BP and ALC_bipolar to show a different perspective of crosstalk. The signals acquired from the FCU were compared with the activation of different muscles. The y-axis displays the SNR values in dB, and thus if the signal is smaller than the baseline, it results in negative values. As can be determined when the targeted muscle was compared with the antagonistic muscle while performing the Radial Deviation movement. Note that the MyoAmpF4F5 recordings were not included.

4.4 Myoelectric Pattern Recognition Accuracy

4.4.1 Offline MPR Accuracy

The offline accuracy for both eEMG and iEMG was computed using the acquired PatRec recordings (Figure 18).

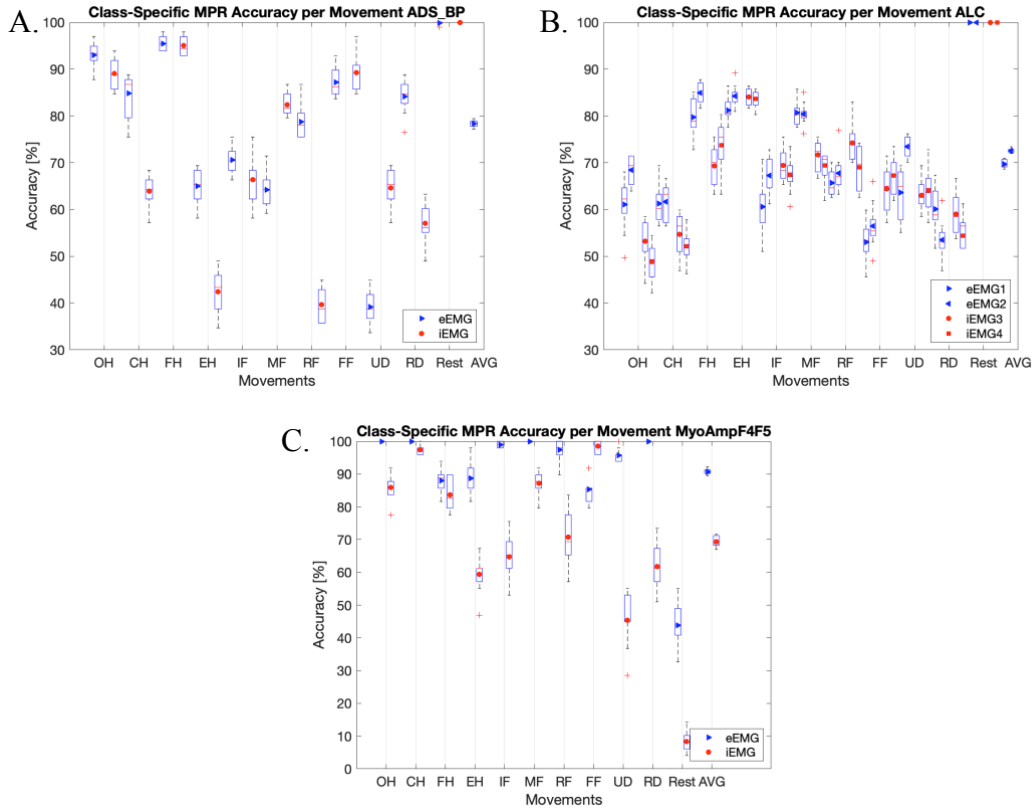

Figure 18 Displays the offline class-specific accuracy obtained from each AFE using the PatRec data from relevant recording sessions. The legend indicates the mean value; the central red line is the median value. The boxplot edges show the 25th, and 75th percentile and the whiskers show the range of values that are not considered as outliers. Outliers are indicated with a red '+' symbol. A. The CS MPR accuracy obtained with the ADS_BP system. B. The CS MPR accuracy obtained with the ALC system. C. The CS MPR accuracy obtained with the MyoAmpF4F5 system

The offline accuracy obtained from the MVC recordings was used to compare the systems collectively, and the error percentage displayed in Figure 19.

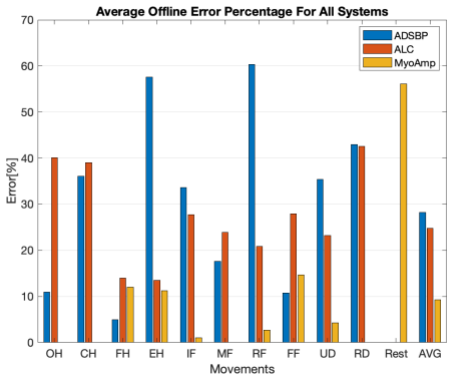

Figure 19 The average offline accuracy displayed as the error percentage [100-Accuracy]. Thus, when no bars are visible, the accuracy was 100%. Note that the MyoAmpF4F5 has a significant error in determining rest.

4.4.2 Real-time MPR Accuracy

The results from the Motion Test (Figure 20), included the real-time accuracy with the associated information on selection time, completion time, and the completion rate acquired by the ADS_BP.

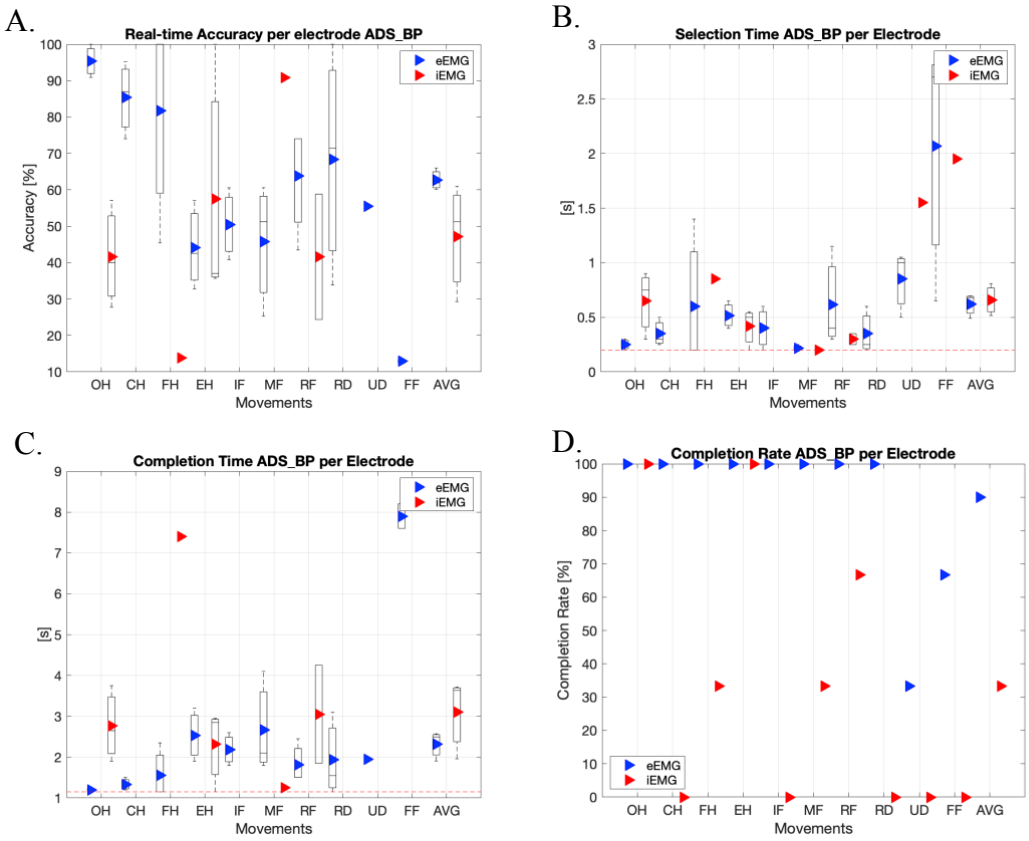

*Figure 20 The result from the Motion Test obtained with ADS_BP from each electrode. A) The real-time accuracy per movement. B) The time it takes to select the movement, the red dotted line shows the minimum time for the algorithm to select the movement. Since the signals are split into 200ms windows with 50ms overlaps, then the least amount of time is 200ms. C) The completion time shows how quickly 20 correct classifications were made; the red dotted line displays the minimum amount of time to reach a decision 200ms + 19*50ms = 1,15s. D) The completion rate displays how often the algorithm can reach the right decision within the time frame given, which was 10s.*

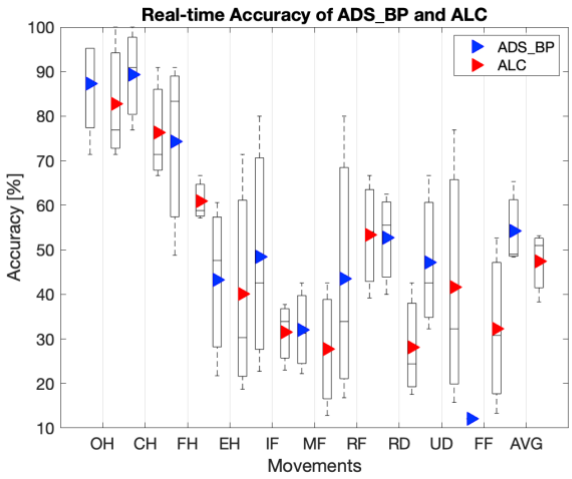

Figure 21 The real-time accuracy between the ADS_BP and the ALC. The boxplot displays the 25th and 75th percentile and the whiskers the standard deviation of the range of the data.

5 Discussion

This chapter is meant to summarize and discuss the main findings and obstacles encountered during the development of this study.

5.1 Problems with a percutaneous interface

Proper attachment of the percutaneous connector needs to be revised for patient comfort, and especially to minimize the strain that can be subjected to the percutaneous wires. A silicone sheath provides a protective layer around the wires of the electrodes. After the placement of the electrodes during surgery, it is essential to validate that the sheaths are covering the wires.

At eleven days post-surgery problems were observed with the impedance measurement. Investigating further fourteen days post-surgery it showed that one electrode was not recording EMG activity. No accident or other misfortune was correlated to this turn of events; however, it was assumed that the wire must have broken because of the percutaneous placement. Due to this, no more recordings were acquired since the objective was to compare both electrodes. On the DOE at Sahlgrenska University Hospital, an X-ray image was taken to see the placement of the electrodes - before the removal surgery. The removal of the bandage revealed that the intramuscular electrode was no longer located within the muscle, but instead it protruded from its original placement. The electrode was, most likely, pulled out via the percutaneous wires or rejected from the muscle. Therefore, the cause of no signal was due to the electrode not being located inside the muscle anymore.

Figure 22 An X-ray image on the DOE. The blue arrow points to the epimysial electrode that was still correctly placed on the muscle. The orange arrow points to the intramuscular electrode, and it displays that the electrode was not where it was supposed to be; the electrode protruded the skin and lay inside the bandages that covered the incisions.

5.2 Comparison and Evaluation

The objective of this study was to compare the eEMG and iEMG electrode types regarding **SNR**, **crosstalk**, and **MPR accuracy**. An additional aspect was comparing the performance of the electrodes between different AFEs.

The RMS peak values were compared between electrodes for selective movements for the ADS_BP and ALC systems. The unexpected similarity between the peak amplitude for the target movement with the implanted muscle and the amplitude in the antagonistic movement (Table 7) requires further analysis.

The **SNR** comparison of the iEMG and eEMG was individually evaluated for ADS_BP and ALC for every movement (Figure 14). For all movements except the Ring Flex obtained by ADS_BP - the eEMG recordings outperformed the iEMG recordings. The iEMG2 contact from the ALC had significantly lower values than the rest of the contacts, which could indicate improper placement of the distal contact of the intramuscular electrode. This consideration might invalidate the finding of eEMG higher SNR values.

Moreover, for the sake of comparison the SNR values were computed also from the MVC recordings. To furtherly enrich the comparison, software-bipolar measurements of the ALC were calculated (Figure 15). For most of the movement classes, the SNR values obtained from the ALC were higher than from the ADS_BP, and, consistently with previously mentioned results, the eEMG provided higher SNR than the iEMG.

Note: Due to complications with the MyoAmpF4F5, the data from MVC recordings were not deemed valid and therefore not included for the MVC-SNR comparison.

The **crosstalk** was evaluated using the cross-correlation function (Equation 2.7). It outputs the correlation value R_{xy} and the higher the value, the more are the similarities between the compared signals. A function R_{xy} equal to 1 indicates zero lag between the autocorrelated signals. The objective was to quantify the crosstalk between the implanted electrodes and the neighboring muscles (Figure 16). It was assumed that the iEMG recordings would produce a lower R_{xy} value, due to the placement inside the targeted muscle.

The values obtained from the ADS_BP and ALC showed similar values (>0.1) when the targeted signal was compared to the different movement classes. From the MyoAmpF4F5, the R_{xy} was close to 1, which indicates that the signals compared were almost identical. This result points out the stronger noise character for this device, which ultimately invalidated these recordings for any reasonable comparison. **Note:** The smallest crosstalk was expected from the FCU vs. rest. However, this was not clear from the graph. Thus, it is suggested to reevaluate these metrics in future studies.

The additional approach to evaluate the crosstalk (Figure 17), did not provide a clear conclusion. The signals produced by the FCU were similar in amplitude as the noise movements, thus dividing the signals as per Equation 2.5 computes a very low number. By converting the results to dB scale a number lower than one outputs a negative number, therefore if the noise is stronger than the signal, the dB value acquired is negative.

The **MPR offline accuracy** used the PatRec recordings to evaluate how effectively the movements were classified per system (Table 8).

Table 8 The average offline CS-MPR accuracy for all systems.

Class-Specific MPR accuracy [%]							
ADS_BP		**ALC**				**MyoAmpF4F5**	
eEMG	**iEMG**	**eEMG1**	**eEMG2**	**iEMG1**	**iEMG2**	**eEMG**	**iEMG**
78,4%	71,8%	69,7%	72,6%	69,4%	68,2%	90,7%	69,4%

The MyoAmpF4F5 CS accuracy showed very high values for the movements but the lowest accuracy for the rest movement. That reveals how misconceiving the offline accuracy can be – therefore, the real-time accuracy MPR accuracy is necessary to determine the usability. An overview of the comparison between the systems (Figure 19) shows how uncorrelated the MyoAmpF4F5 recordings are compared to the ADS_BP and ALC.

The **MPR real-time accuracy** was obtained by using the Motion Test and the recordings were obtained with the ADS_BP to compare the two electrode types and not to compare systems (Figure 20). The eEMG produced higher accuracy, the average 62.7% for eEMG and 47.2% for iEMG.

The selection time and completion time between the electrodes were consistent, but as can be shown the completion rate for the eEMG is significantly higher than for the iEMG.

Out of interest, the ADS_BP and ALC systems were compared to the averaged real-time MPR accuracy, and the results showed that the ADS_BP had an average accuracy of 54.3% and the ALC 47.5%.

5.3 Recordings

The GUI in BioPatRec provided valuable information during the recording sessions and offered the possibility to repeat the movement if any undesired artifacts were visualized. However, when the different AFEs were compared, it displayed significant differences. E.g., the recordings from the ADS_BP and MyoAmpF4F5 seemed to be inverted (Figure 23). Due to time limitations and that it exceeded the scope for this thesis, the reasoning behind this was not obtained. Note that all connections were doubled checked to assure that everything was connected properly.

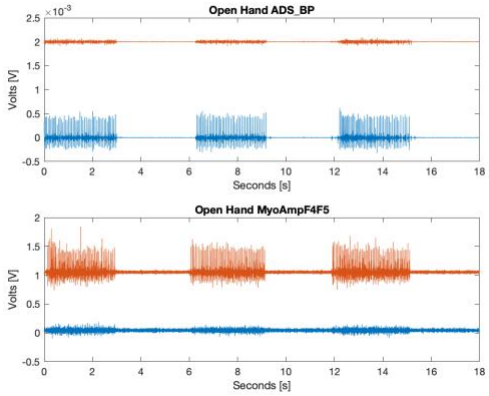

Figure 23 Performing open hand movement with the ADS_BP and the MyoAmpF4F5 systems. The blue and red graphs were eEMG and iEMG recordings, respectively. The x-axis was shifted to distinguish the two signals easily.

It was notable that the volunteer was not able to always maintain MVC during the 3-second contraction (Figure 24), where the initial samples show a larger amplitude as to the rest of the recording.

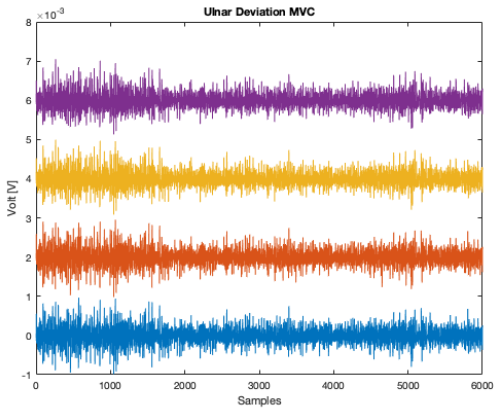

Figure 24 MVC recording while performing the ulnar deviation movement.

The recordings with the MyoAmpF4F5 proved to be challenging. The recordings were subjected to a significant amount of noise while performing the movements with the adjacent muscles and the antagonistic movement (Figure 25).

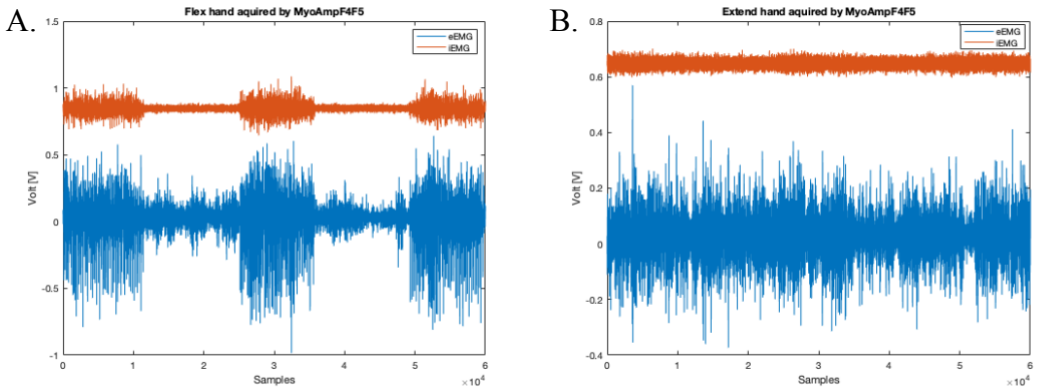

Figure 25 PatRec recordings obtained with the MyoAmpF4F5. A. The flex hand movement. B. The extend hand movement

5.4 Limitations

The scope of this thesis was limited to implantable muscle-based electrodes, where the EMG signals were obtained from one muscle of one able-bodied volunteer.

In this study, the movements were selected in an attempt to activate specific muscles selectively. In general, it is objectively challenging to activate single muscle selectively. Indeed, analyzing the results revealed that, most likely, for some movements single muscle activation was not reached.

Different placements of the implanted electrodes result in different stresses on the design. Epimysial electrodes are located outside the muscle; therefore, it is submitted to less mechanical stress than the intramuscular electrode, which could result in a longer lifetime of these electrodes. This was not considered in the scope of this thesis.

The cross-correlation function for the evaluation of crosstalk has been reported to be an insufficient measure for that evaluation [43]. In the literature, this is still the most common way, and no alternatives are available; therefore, it was deemed as a comparison metric for this thesis. A different approach shall be considered since the results presented were inconclusive.

5.5 Future Work

For future work on this comparison, a few obstacles need to be overcome. Firstly, an implanted reference under the skin is required, so the different impedance between the implanted electrodes and the reference is not as significant. That modification could potentially solve the problems with the ADS_BP and the MyoAmpF4F5. This will need to be addressed before continuing collecting the data.

The MyoAmpF4F5 circuit needs to be re-evaluated and the gain adjusted for optimal results. It has a variable gain from 50-5000, and for this study, the gain of approximately 500 was used without exploring other options. Problems related to the amplitude of the noise will need to be addressed. It seemed as the amplitude of the signals had to reach a certain threshold above the noise level to trigger visible contractions among the noise, the strong contractions thus managed to scale the noise level down. For the lower amplitude noise induced movements the amplitude did not manage to reach that threshold.

The intramuscular electrodes must be secure in place by an anchoring mechanism and sutures to prevent from migrating out of the muscle.

It is essential to recruit more volunteers to determine the statistical significance of the electrodes comparison.

The possibility of using electrical stimulation should be explored to try to isolate the EMG signals to the muscles of interest.

6 Conclusion

The main objective of this study was to compare the SNR values acquired by each muscle-based electrode. The eEMG electrodes provided slightly higher SNR than the corresponding iEMG recordings. The values varied between the systems that acquired the signals, but the eEMG performed consistently better. The remaining objectives used as performance metrics for this comparison revealed that the crosstalk between the adjacent muscles was inconclusive. The MPR accuracy for both offline and real-time performance revealed that on average, the eEMG outperformed the iEMG. The comparison within the acquisition systems regarding MPR accuracy deemed the ADS_BP as the best performing. The developed framework is potentially suitable for further research in additional subjects. Further work using the methods developed is essential to reach conclusive results.

Appendix I

Simplified electrical diagrams three AFEs used.

ADS_BP

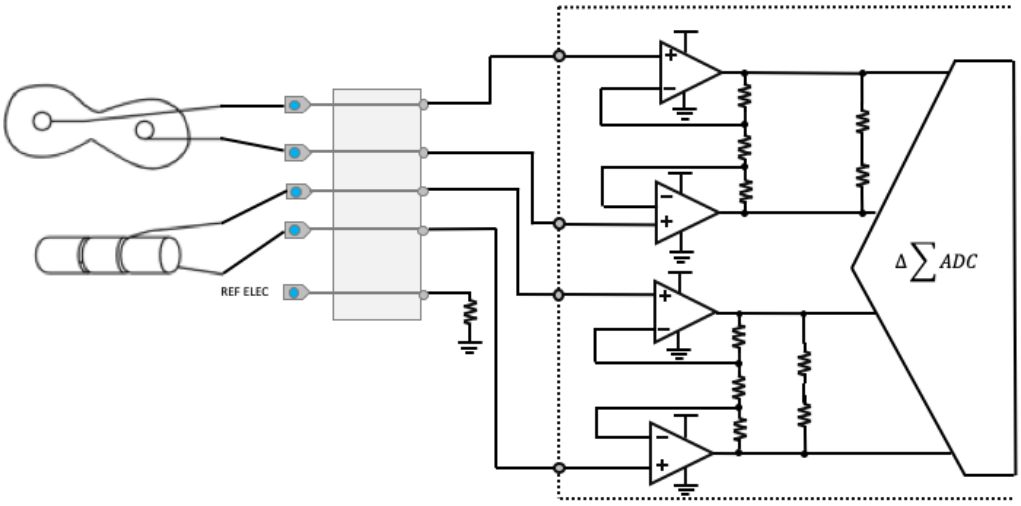

ALC

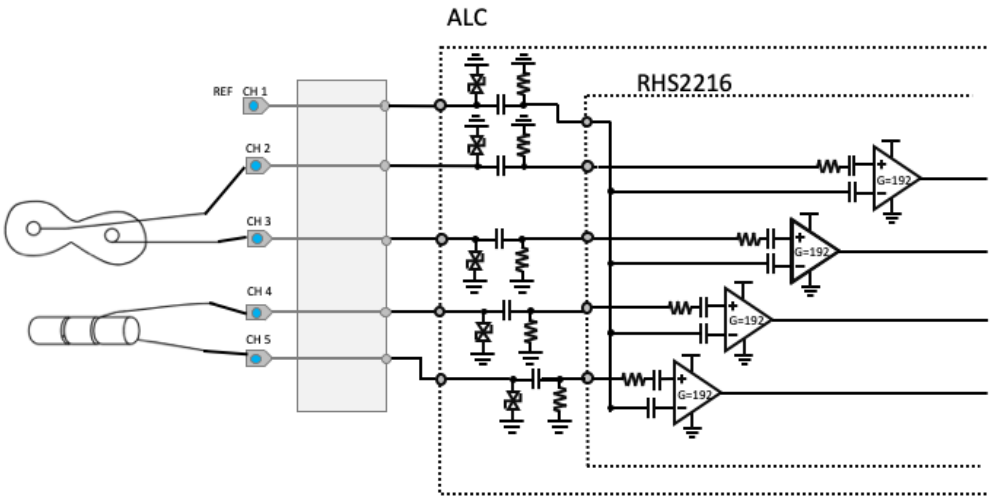

MyoAmpF4F5

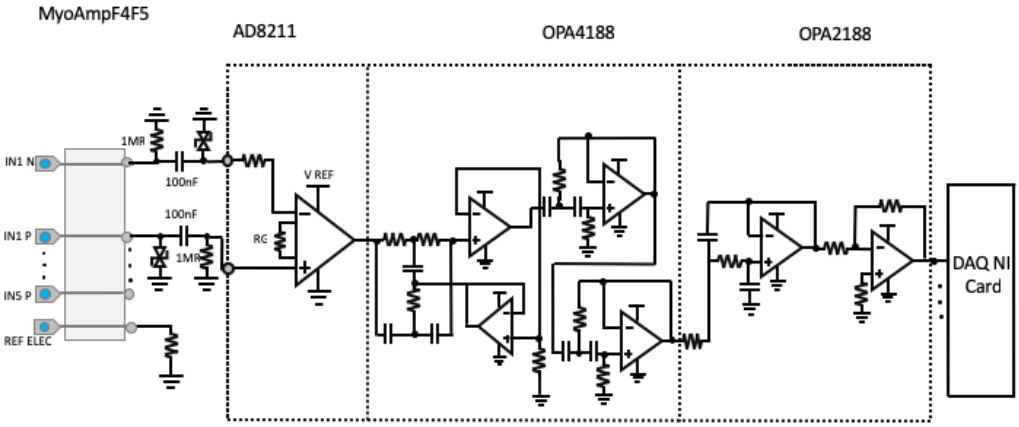
MyoAmpF4F5
AD8211
OPA4188
OPA2188
IN1 N
IN1 P
IN5 P
REF ELEC
1MR
100nF
100nF
1MR
RG
V REF
DAQ NI
Card

References

[1] K. Ziegler-Graham, E. J. MacKenzie, P. L. Ephraim, T. G. Travison, and R. Brookmeyer, "Estimating the Prevalence of Limb Loss in the United States: 2005 to 2050," *Arch. Phys. Med. Rehabil.*, vol. 89, no. 3, pp. 422–429, 2008.

[2] M. Ortiz-Catalan, R. Brånemark, B. Håkansson, and J. Delbeke, "On the viability of implantable electrodes for the natural control of artificial limbs: Review and discussion," *Biomed. Eng. Online*, vol. 11, 2012.

[3] M. Ortiz-Catalan, N. Sander, M. B. Kristoffersen, B. Håkansson, and R. Brånemark, "Treatment of phantom limb pain (PLP) based on augmented reality and gaming controlled by myoelectric pattern recognition: A case study of a chronic PLP patient," *Front. Neurosci.*, vol. 8, no. 8 FEB, pp. 1–7, 2014.

[4] M. Ortiz-Catalan, B. Håkansson, and R. Brånemark, "Real-time and simultaneous control of artificial limbs based on pattern recognition algorithms," *IEEE Trans. Neural Syst. Rehabil. Eng.*, vol. 22, no. 4, pp. 756–764, 2014.

[5] K. J. Zuo and J. L. Olson, "The evolution of functional hand replacement: From iron prostheses to hand transplantation," *Can. J. Plast. Surg.*, vol. 22, no. 1, pp. 44–51, 2014.

[6] R. Brånemark, Ö. Berlin, K. Hagberg, P. Bergh, B. Gunterberg, and B. Rydevik, "A novel osseointegrated percutaneous prosthetic system for the treatment of patients with transfemoral amputation: A prospective study of 51 patients," *Bone Jt. J.*, vol. 96 B, no. 1, pp. 106–113, 2014.

[7] P. I. Brånemark, U. Breine, R. Adell, B. O. Hansson, J. Lindström, and A. Ohlsson, "Intra-osseous anchorage of dental prostheses: I. Experimental studies," *Scand. J. Plast. Reconstr. Surg. Hand Surg.*, vol. 3, no. 2, pp. 81–100, 1969.

[8] Y. Li and R. Brånemark, "Osseointegrated prostheses for rehabilitation following amputation," *Unfallchirurg*, vol. 120, no. 4, pp. 285–292, Apr. 2017.

[9] C. K. Battye, A. Nightingale, and J. Whillis, "The Use of Myo-Electric Currents in the Operation Of Prostheses," *J. Bone Joint Surg. Br.*, vol. 37-B, no. 3, pp. 506–510, 1955.

[10] R. W. Wirta, D. R. Taylor, and F. R. Finley, "Pattern Recognition Arm Prosthesis: A historical perspective - A final report," *Bull. Prosthes. Res*, pp. 8–

35, 1978.

[11] K. Englehart, B. Hudgins, P. . Parker, and M. Stevenson, “Classification of the myoelectric signal using time-frequency based representations,” *Med. Eng. Phys.*, vol. 21, no. 6–7, pp. 431–438, Jul. 1999.

[12] M. Ortiz-Catalan, F. Rouhani, R. Branemark, and B. Hakansson, “Offline accuracy: A potentially misleading metric in myoelectric pattern recognition for prosthetic control,” *Proc. Annu. Int. Conf. IEEE Eng. Med. Biol. Soc. EMBS*, vol. 2015-Novem, pp. 1140–1143, 2015.

[13] W. M. Grill, “Selective activation of the nervous system for motor system neural prostheses,” in *Intelligent systems and technologies in rehabilitation engineering.*, L. C. Horia-Nicolai LT, Ed. 2001, pp. 209–241.

[14] J. Perry, C. Schmidt Easterday, and D. J. Antonelli, “Surface versus intramuscular electrodes for electromyography of superficial and deep muscles,” *Phys. Ther.*, vol. 61, no. 1, pp. 7–15, 1981.

[15] L. H. Smith and L. J. Hargrove, “Comparison of surface and intramuscular EMG pattern recognition for simultaneous wrist/hand motion classification,” *Proc. Annu. Int. Conf. IEEE Eng. Med. Biol. Soc. EMBS*, pp. 4223–4226, 2013.

[16] T. Farrell and R. Weir, “A Comparison of the Effects of Electrode Implantation and Targeting on Pattern Classification Accuracy for Prosthesis Control,” *IEEE Trans. Biomed. Eng.*, vol. 55, no. 9, p. 2198, 2008.

[17] L. J. Hargrove, K. Englehart, and B. Hudgins, “A comparison of surface and intramuscular myoelectric signal classification,” *IEEE Trans. Biomed. Eng.*, vol. 54, no. 5, pp. 847–853, 2007.

[18] W. D. Memberg, P. H. Peckham, and M. W. Keith, “A Surgically-Implanted Intramuscular Electrode for an Implantable Neuromuscular Stimulation System,” *IEEE Trans. Rehabil. Eng.*, vol. 2, no. 2, pp. 80–91, 1994.

[19] I. C. Sando *et al.*, “Regenerative Peripheral Nerve Interface for Prostheses Control: Electrode Comparison,” *J. Reconstr. Microsurg.*, vol. 32, no. 3, pp. 194–199, 2016.

[20] W. D. Memberg, T. G. Stage, and R. F. Kirsch, “A fully implanted intramuscular bipolar myoelectric signal recording electrode,” *Neuromodulation*, vol. 17, no. 8, pp. 794–799, 2014.

[21] M. Ortiz-Catalan, B. Håkansson, and R. Brånemark, “An osseointegrated human-machine gateway for long-term sensory feedback and motor control of

artificial limbs," *Sci. Transl. Med.*, vol. 6, no. 257, 2014.

[22] E. Mastinu, P. Doguet, Y. Botquin, B. Hakansson, and M. Ortiz-Catalan, "Embedded System for Prosthetic Control Using Implanted Neuromuscular Interfaces Accessed Via an Osseointegrated Implant," *IEEE Trans. Biomed. Circuits Syst.*, vol. 11, no. 4, pp. 867–877, 2017.

[23] R. L. Drake, A. Wayne Vogl, and A. W. . Mitchell, *Gray's Anatomy for Students*. 2015.

[24] A. Barbero, M. and Merletti, R. and Rainoldi, *Atlas of Muscle Innervation Zones: Understanding Surface Electromyography and Its Applications*. Springer Milan, 2012.

[25] I. Rodriguez-Carreno, L. Gila-Useros, and A. Malanda-Trigueros, "Motor Unit Action Potential Duration: Measurement and Significance," in *Advances in Clinical Neurophysiology*, vol. 2, InTech, 2012, pp. 137–164.

[26] C. J. De Luca, A. Adam, R. Wotiz, L. D. Gilmore, and S. H. Nawab, "Decomposition of Surface EMG Signals," *J. Neurophysiol.*, vol. 96, no. 3, pp. 1646–1657, 2006.

[27] E. Mastinu, R. Poli, and L. Citi, "Crosstalk Reduction in Epimysial EMG Recordings from Transhumeral Amputees with Principal Component Analysis," 2018, pp. 2124–2127.

[28] E. Mastinu, M. Ortiz-Catalan, and B. Hakansson, "Analog Front-Ends comparison in the way of a portable, low-power and low-cost EMG controller based on pattern recognition EMBC 2015," in *Proceedings of the Annual International Conference of the IEEE Engineering in Medicine and Biology Society, EMBS*, 2015, vol. 2015-Novem, pp. 2111–2114.

[29] M. Ortiz-Catalan, R. Brånemark, and B. Håkansson, "BioPatRec: A modular research platform for the control of artificial limbs based on pattern recognition algorithms," *Source Code Biol. Med.*, 2013.

[30] A. M. Simon, L. J. Hargrove, B. A. Lock, T. A. Kuiken, and A. Simon, "The Target Achievement Control Test: Evaluating real-time myoelectric pattern recognition control of a multifunctional upper-limb prosthesis," 2011.

[31] T. A. Kuiken, B. A. Lock, R. D. Lipschutz, L. A. Miller, K. A. Stubblefield, and K. B. Englehart, "Targeted Muscle Reinnervation for Real-time Myoelectric Control of Multifunction Artificial Arms," *J. Am. Med. Assoc.*, vol. 301, no. 6, pp. 619–628, 2016.

[32] J. P. M. Mogk and P. J. Keir, “Crosstalk in surface electromyography of the proximal forearm during gripping tasks,” *J. Electromyogr. Kinesiol.*, vol. 13, no. 1, pp. 63–71, Feb. 2003.

[33] T. R. Farrell and R. F. ff Weir, “A comparison of the effects of electrode implantation and targeting on pattern classification accuracy for prosthesis control,” *IEEE Trans. Biomed. Eng.*, vol. 55, no. 9, pp. 2198–2211, 2008.

[34] E. Mastinu, J. Ahlberg, E. Lendaro, L. Hermansson, B. Hakansson, and M. Ortiz-Catalan, “An Alternative Myoelectric Pattern Recognition Approach for the Control of Hand Prostheses: A Case Study of Use in Daily Life by a Dysmelia Subject,” *IEEE J. Transl. Eng. Heal. Med.*, vol. 6, 2018.

[35] K. Sugie *et al.*, “Characteristic MRI findings of upper limb muscle involvement in myotonic dystrophy type 1,” *PLoS One*, vol. 10, no. 4, 2015.

[36] M. A. Mahan, J. Gasco, D. B. Mokhtee, and J. M. Brown, “Anatomical considerations of fascial release in ulnar nerve transposition: a concept revisited,” *J. Neurosurg.*, vol. 123, no. 5, pp. 1216–1222, 2015.

[37] E. Mastinu, “Towards clinically viable neuromuscular control of bone-anchored prosthetic arms with sensory feedback,” Chalmers University of Technology, 2019.

[38] I. Technologies, “RHS2116 Digital Electrophysiology Stimulator / Amplifier Chip,” 2018.

[39] E. Mastinu, B. Håkansson, and M. Ortiz-catalan, “Low-cost , open source bioelectric signal acquisition system,” pp. 12–15, 2017.

[40] Texas Instruments, “ADS1299-x Low-Noise, 4-, 6-, 8-Channel, 24-Bit, Analog-to-Digital Converter for EEG and Biopotential Measurements,” 2017.

[41] NI, “DAQ M Series - NI USB-621x User Manual,” no. April. p. 204 p., 2009.

[42] M. Ortiz-Catalan, R. Brånemark, and B. Håkansson, “BioPatRec: A Modular Research Platform for Prosthetic Control Algorithms Based on Bioelectric Pattern Recognition,” *Source Code Biol. Med.*, vol. 8, no. 11, pp. 1–18, 2013.

[43] M. M. Lowery, N. S. Stoykov, and T. A. Kuiken, “A simulation study to examine the use of cross-correlation as an estimate of surface EMG cross talk,” *J. Appl. Physiol.*, vol. 94, no. 4, pp. 1324–1334, Apr. 2003.